ELSEVIER

Sedimentary Geology 152 (2002) 133–158

Sedimentary Geology

www.elsevier.com/locate/sedgeo

Late Quaternary incised-valley fill of the Yangtze delta (China): its stratigraphic framework and evolution

Congxian Li [a], Ping Wang [b,*], Heping Sun [a], Jiaqiang Zhang [a], Daidu Fan [a], Bing Deng [a]

[a] *Marine Geology Laboratory, Tongji University, Shanghai 200092, People's Republic of China*
[b] *Department of Geology, University of South Florida, 4202 East Flower Avenue, SCA 528, Tampa, FL 33620, USA*

Received 30 July 2001; accepted 26 November 2001

Abstract

A Late Quaternary stratigraphic framework of the Yangtze delta, China, has been established based on the analysis and correlation of over 600 cores. Thirty cores were drilled and analyzed during this study, and the rest were collected from numerous publications. The Late Quaternary stratigraphic framework of the Yangtze delta consists of incised-valley fill and two interfluvial sequences. The incised valley roughly coincides with the modern Yangtze delta. From bottom to top, the incised-valley fill sequence is typically composed of channel, floodplain–estuary, estuary–shallow marine, and modern deltaic facies. The interfluvial sequences occur along the two flanks of the incised-valley fill. On the southern flank, seaward of the maximum-transgression line, the interfluvial sequence is typically composed of marsh–nearshore, shallow marine, and tidal flat facies with predominantly muddy deposits. On the northern flank, the interfluvial sequence is typically composed of barrier–lagoon, tidal sand ridge, and littoral–tidal flat facies with predominantly sandy deposits. The interfluvial sequence landward of the maximum-transgression line on both flanks is composed mainly of lacustrine muddy deposits. The post-glacial fining-upward incised-valley fill sequence was formed by retrogressive aggradation in the lower reach of the Yangtze River, induced by sea-level rise. The upstream extent of the retrogressive aggradation exceeds the reach of flood tidal currents, which explains the lack of marine fossil and tidal sedimentary structures in the channel sand deposits. A huge estuary was formed in the present Yangtze delta area when the post-glacial transgression reached maximum at about 7500 years BP. The shallow marine mud was deposited broadly in the estuary and the maximum flooding surface, which separates the underlying transgressive sequence from overlying regressive sequence, located within the muddy stratum. An erosional surface between the channel sand unit and deltaic sand unit exists at the apical area of the Yangtze delta. The modern Yangtze delta developed after the post-glacial transgression maximum was reached. The delta development was dominated by the abundant fluvial sediment supply. Six sub-deltas with a southward migrating trend have developed.

Keywords: Yangtze delta; China; Incised-valley system; Late Quaternary; Stratigraphic framework; Retrogressive aggradation; Post-glacial transgression

1. Introduction

The Yangtze (Changjiang) delta, China, is one of the world's major deltas with dense population and tremendous economical developments. Information about the Yangtze delta, particularly in the aspect of Late

* Corresponding author. Tel.: +1-813-974-9170; fax: +1-813-974-2654.
E-mail addresses: cxlik@online.sh.cn (C. Li), pwang@chuma1.cas.usf.edu (P. Wang).

0037-0738/02/$ - see front matter
PII: S0037-0738(02)00066-0

Quaternary stratigraphy, is relatively scarce in the scientific literature as compared to some of the well-documented large deltas, such as the Mississippi delta (Russell and Russell, 1939; Wright and Coleman, 1972; 1988; Roberts, 1997; Coleman et al., 1998) and the Nile delta (Said, 1981; Stanley, 1996; Stanley and Bernasconi, 1998; Stanley and Warne, 1998).

One of the original descriptions of an incised-valley system was established by Fisk (1944) and Fisk and McFarlan (1955) in the Mississippi River. Fisk and McFarlan (1955) were also among the first to describe the relationship between the incision and filling of the Mississippi trench (valley) with the falling and rising of sea level. Incised-valley systems have been studied in various places, e.g., along the Texas and Louisiana coasts (Wilkinson and Byrne, 1977; Suter et al., 1987; Nichol et al., 1996), along the Delaware coasts (Belknap and Kraft, 1985), and along the Australian New South Wales coast (Roy, 1984, 1994; Roy et al., 1995). Incised-valley systems have been interpreted throughout geological history, from Precambrian to the Quaternary (Fisk, 1944; Fisk and McFarlan, 1955; Oomkens, 1970, 1974; Wilkinson and Byrne, 1977; Li 1985; Li et al., 1988; Allen and Posamentier, 1993; Dalrymple et al., 1994; Zhang and Li, 1996; Gupta, 1997, 1999). Incised valleys may be developed in both loose sediment and bedrock (Fisk, 1944; Roy 1994; Nichol et al., 1996, 1997; Gupta 1997, 1999). It has been realized during the development of sequence stratigraphy that recognition of incised-valley system provides an important criterion for the identification of sequence boundaries (e.g., Posamentier and Vail, 1988; Van Wagoner et al., 1988, 1990). As a consequence, there have been numerous studies recently on incised-valley systems (e.g., Allen and Posamentier, 1993; Dalrymple and Zaitlin, 1994; Dalrymple et al., 1992, 1994). Two types of incised-valley system have been identified: piedmont incised-valley system and coastal plain incised-valley system (Zaitlin et al., 1994). Three longitudinal segments describing the different degrees of marine and fluvial influences, and the associated stratigraphic sequences in each segment in response to the rise and fall of base level were distinguished (Dalrymple et al., 1994; Zaitlin et al., 1994). Estuarine deposits are key components of incised-valley fill and are typically subdivided into bay head, central basin and bay-mouth (wave-dominated or tide-dominated) facies (Dalrymple et al., 1992, 1994; Roy, 1994; Roy et al., 1995; Nichol et al., 1996, 1997). It is generally comprehended that paleo-valley incision is controlled by sea-level fall, while sea-level rise and abundant sediment supply lead to the fill of incised valleys (Fisk and McFarlan, 1955; Zaitlin et al., 1994; Li et al., 2000). Backstepping aggradation is emphasized as a key process in the fill of incised valleys (Gupta, 1997, 1999).

Numerous cores were drilled in the Yangtze delta area during the last four decades, providing a solid database for understanding its stratigraphic framework (Fig. 1). More than 600 cores, including 30 drilled and analyzed during this study, were examined. Samples from the 30 cores were examined in detail, including sedimentological, lithological, and paleontological analyses. These 30 cores served as regional controls for the stratigraphic correlation. Four types of facies assemblages were classified in the cores. Six sections, including three roughly perpendicular to the coastline (latitudinal) and three parallel to the coastline (longitudinal), were described. A Late Quaternary stratigraphic framework for the Yangtze delta was established based on the analyses of cores and transects.

The geomorphology, hydrology, and sedimentary characteristics of the Yangtze delta have been documented (e.g., Chen and Stanley 1993, 1995; Stanley and Chen, 1993; Chen and Chen, 1997; Chen, 1998). However, a Late Quaternary stratigraphic framework of the entire subaerial Yangtze delta has not been established. The objectives of this study were: (1) to develop a Late Quaternary stratigraphic framework for the Yangtze delta; (2) to discuss the Late Pleistocene evolution of Yangtze delta; and (3) to identify distinctive features in the development of the Yangtze delta.

2. Study area

Yangtze River, the longest river in China, originates from the Qinhai–Tibet Plateau and discharges into the East China Sea in a tectonic subsidence belt (Li et al., 1991). The 1.8×10^6 km^2 drainage basin spans an elevation difference of over 4000 m, and is strongly influenced by the monsoons. The tremendous elevation drop, being one of the major high-mountain rivers, and abundant precipitation result in enormous

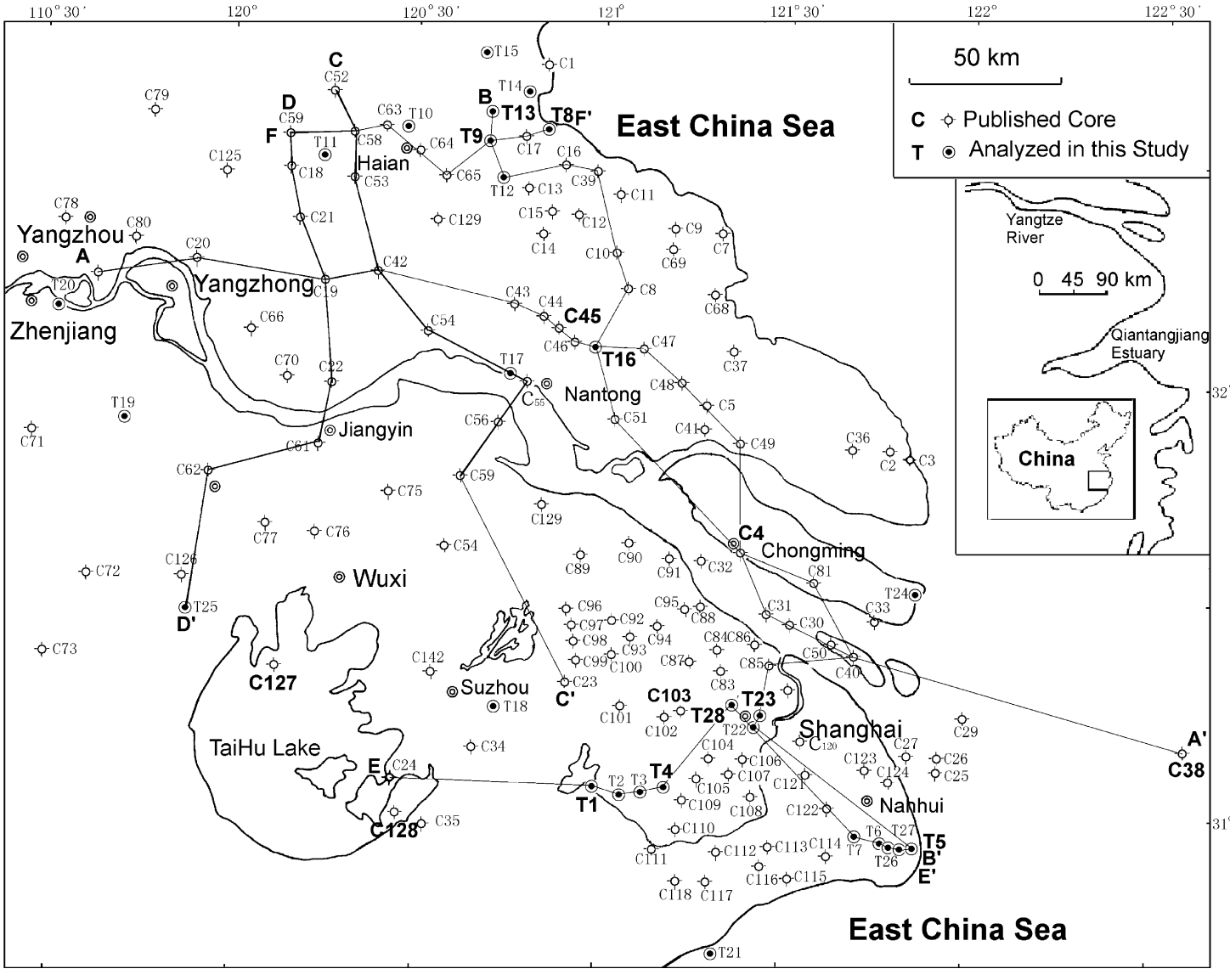

Fig. 1. Locations of key cores and stratigraphic sections. Bold labels indicate the cores that are illustrated in this paper.

water and sediment discharges, which average 5.0×10^{11} kg and 924 km^3 annually (Milliman and Meade, 1983; Li et al., 1991; Milliman and Syvitski, 1992). The great elevation drop and tremendous water discharge provide strong driving forces for the valley incision, while the rich sediment supply provides the potential for rapid valley fill.

The Yangtze River enters the eastern plain from the hilly area in the vicinity of Zhejiang–Yangzhou area, forming the Holocene delta (Fig. 2). The Holocene Yangtze delta covers an area of approximately 52,000 km^2, with 23,000 km^2 subaerial and 29,000 km^2 subaqueous. The ratio of the subaerial and subaqueous portions is 0.79 (Li et al., 1979; Li and Li, 1983; Li, 1986). The Yangtze River mouth is influenced by semidiurnal tide with an average range of 2.6 m. The spring tidal range can reach as high as 4.5 m, generating tidal currents of up to 1.0–1.5 m/s in the distributaries (Chen, 1998). Water-level fluctuations attributable to tides are measured up to 624 km upstream from the river mouth. The flood tidal current was measured up to the Yangzhong area, east of the delta apex, some 230 km upstream from the river mouth during dry season spring tides (Fig. 1). During the rainy season, flood tidal current was measured roughly 150 km upstream from the river mouth, around the Jiangyin area (Li et al., 1983). The tidal range along the northern flank of the modern Yangtze delta is generally greater than that along the southern flank (Qian et al., 1964; Ren, 1986; Chen, 1998).

There have been six stages of mouth-bar development in the Holocene Yangtze delta (Fig. 2), identified on the basis of core analysis (Li and Li, 1983; Li, 1984). The main distributary of each delta-development stage has tended to migrate southward during the last 7500 years (Li, 1984, 1986; Chen and Stanley, 1995). The present Yangtze River mouth is divided by three active mouth bars into four distributaries, continuing the same trend since the post-glacial maximum.

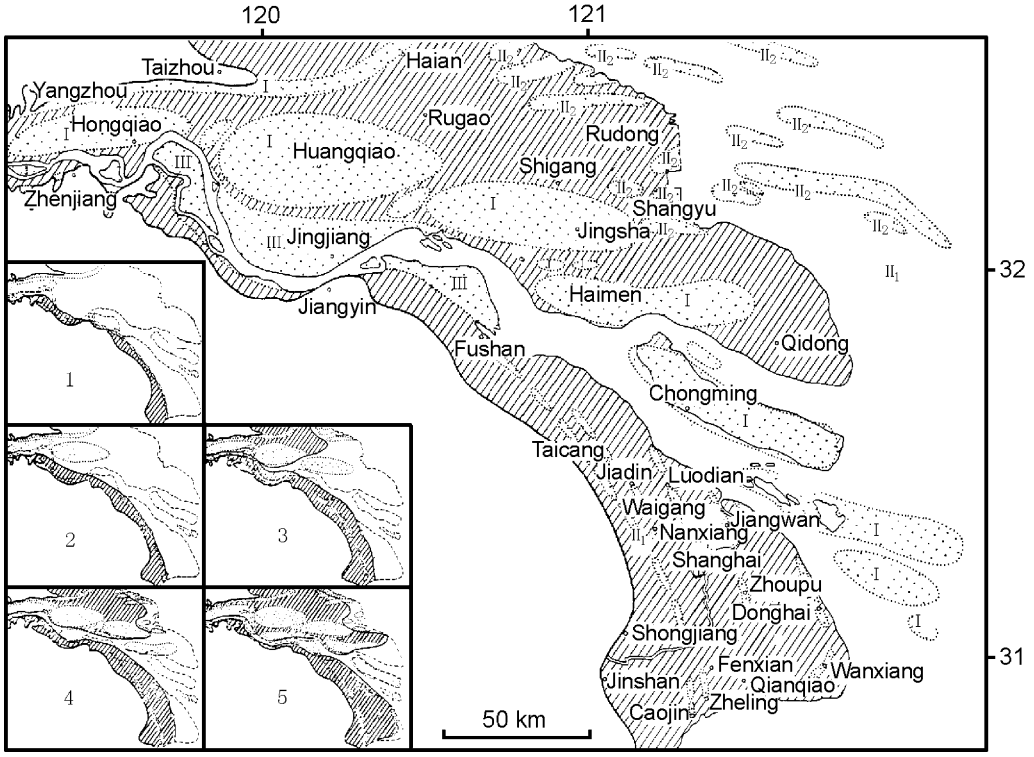

Fig. 2. Six stages of mouth bar development in the Yangtze delta, with stage 6 enlarged. See Fig. 1 for regional location. I: Mouth sand bar; II: marine sand body; II_1: chenier and longshore bar; II_2: tidal sand ridge; III: fluvial sand body (after Li and Li, 1983).

The apex of the Holocene Yangtze delta is located in Zhenjiang–Yangzhou area, approximately 250 km west of the modern river mouth. The Yangtze delta was divided into three major units: the main delta body (I), the southern (II) and the northern (III) flanks (Fig. 3). The two flanks were further divided into two zones (II_1, II_2 and III_1, III_2), respectively, along the line of post-glacial transgression maximum. The entire Yangtze delta is located in the coastal subsidence zone (Li et al., 1991). The subsidence rate ranges from 1 to 3 mm/year (Stanley and Chen, 1993; Chen and Stanley, 1993, 1995; Chen, 1998) and decreases toward the west. The hilly region (IV) west of the delta area is a tectonic uplift zone, and is separated from the coastal subsidence zones by the approximately north–south hinge line located along Zhenjiang area.

Sea level in the East China Sea was at 110–130 m below present mean level from 18–21 ky BP (1 ky = 1000 years) (Saito, 1998). Rapid sea-level rise, with an average rate of 1.0–1.2 cm/year, was measured until approximately 7 ky BP (Fig. 4). Since 7 ky BP, the rate of sea-level rise has decelerated considerably, with an average rate ranging from 0.28 to 0.52 cm/year in the Yangtze delta area (Li and Ming, 1981). It is worth noting that since 7 ky BP, sea level has

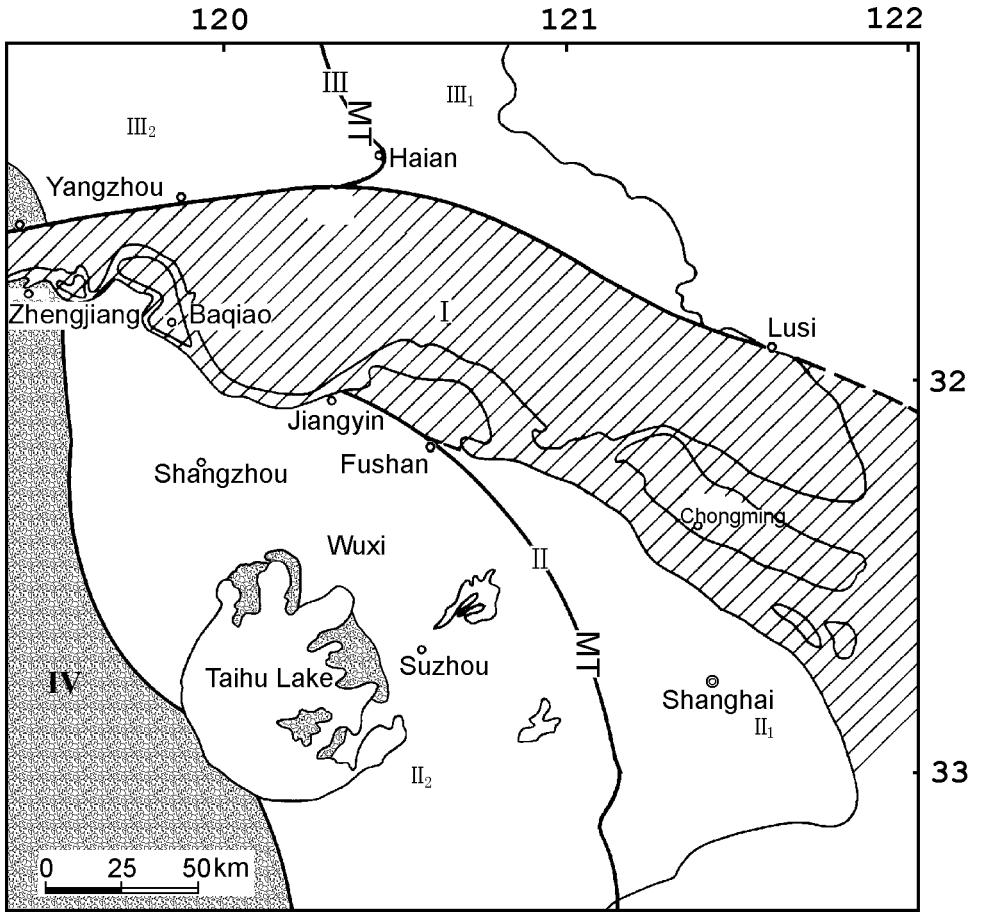

Fig. 3. Delta main body and the two flanks. MT: Limit of post-glacier maximum transgression. See Fig. 1 for regional location. I: Delta main body; II: southern flank; II_1: seaward of MT; II_2: landward of MT (Taihu Lake area) with some separated hills; III: northern flank; III_1: seaward of MT; III_2: landward of MT; IV: hilly area.

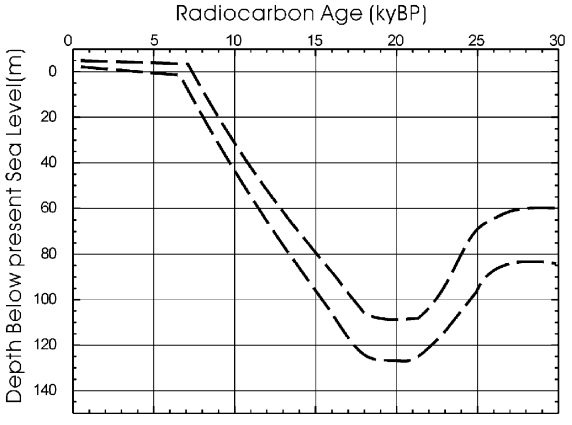

Fig. 4. Schematic Late Quaternary sea-level change curve in the East China Sea; 1 ky = 1000 years (after Saito, 1998).

reached the study area. The 0.28–0.52 cm/year rate was obtained from the study area, and is different from that of the East China Sea rate shown in Fig. 4.

3. Methodology

The present study is based primarily on facies analysis and stratigraphic correlation of over 600 cores. An example of the comprehensive core analyses is illustrated in Fig. 5. Most of the cores were drilled and sampled with a rotational device with a diameter of either 56 or 108 mm. The cores were typically drilled to a depth of 30–50 m, with approximately 15% reaching 200–300 m deep. The recovery rate in the sand and mud layers ranged from 50% to 60% and 60 to 70%, respectively. A piston drill with a recovery rate of approximately 80% to even 90% was used for the remainder of the cores. Thirty cores at key locations were drilled and analyzed specifically for this study. The cores were split in half, and following core description, sediment samples were collected from one half, while the other half was stored as repository.

Core description includes color, texture, lithology, macrofossil assemblages, bioturbation features, and sedimentary structures. Grain-size analysis was conducted based on Folk (1974) method using a combination of sieving (for sand and coarser fractions) and pipette (for silt and clay fractions). Heavy-minerals were identified under a microscope and their composition was obtained based on the counting of more than 300 grains. Microfossil assemblages were examined from 50 g of dry sediment samples using the method described by Wang (1985).

Interpretations of depositional environments were based on a combination of field observation at the drilling site and core sample analyses outlined above. Depositional energy was estimated based primarily on grain size, sedimentary structure, and heavy-mineral composition. Degrees of marine influence were determined based largely on microfossil assemblages, especially those of foraminifers. Micro-morphological analyses were applied to identify and characterize the paleosol (Li et al., 1996, 2000; Chen, 1997; Deng et al., 1999). Limited geophysical well-logs, mostly resistivity logs, were used to distinguish some facies, mostly toward the upstream where saltwater influence is minimal.

The concept of sequence stratigraphy, particularly pertaining to the understanding of the origin and fill of incised-valley systems (Posamentier et al., 1988; Posamentier and Vail, 1988; Van Wagoner et al., 1988, 1990), was applied to establish the Late Quaternary stratigraphic framework. The stratigraphic correlation was based primarily on the sequence boundary, maximum flooding surface, and transgressive and regressive successions, instead of lithology or depositional environments.

4. Facies description and interpretation

Eleven sedimentary facies were distinguished and described based on the core sample analyses (Table 1). The sequence in which each of these facies is described and interpreted does not reflect their order of occurrence in the stratigraphic record. The lateral and vertical distributions of these facies are discussed in the following section.

4.1. River channel facies

This facies, the coarsest in the entire area, is composed of medium to fine sands with cross-bedding. Gravels, of typically 0.3–0.5 cm in diameter, were found near the bottom, although they generally ac-

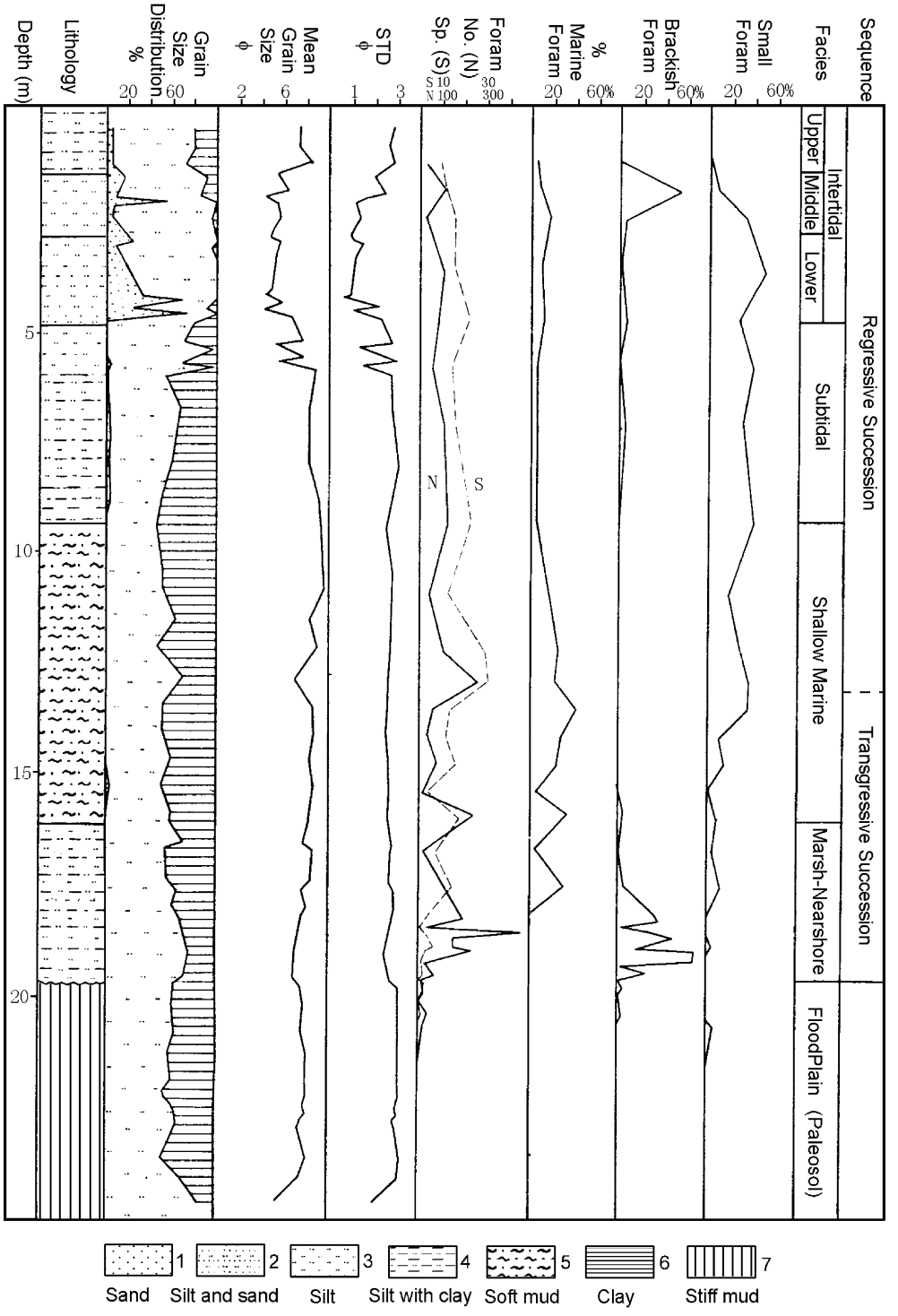

Fig. 5. Type 1 facies assemblage illustrated by core T23. Column 6 indicates number of individual foraminifer (*N*) and number of species (*S*) in 50 g of dry sample. STD is the abbreviation of standard deviation.

Table 1
Facies assemblages and characteristics in various parts of the Yangtze delta

Location	Text section	Genetic unit	Lithology
Incised valley	Section 4.1	River channel	Sand and sand with gravel
	Section 4.2	Floodplain–estuary	Sandy clay with sand lenses
	Section 4.3	Estuary–prodelta	Soft mud
	Section 4.4	Delta	Clayey sand and sandy clay
Southern flank			
II_1	Section 4.5	Terrestrial (floodplain facies, basement)	Stiff clay
	Section 4.6	Marsh–nearshore	Silty clay
	Section 4.7	Shallow marine	Soft mud
	Section 4.8	Tidal flat	Silty clay and clayey silt
II_2	Section 4.9	Lacustrine	Mud with peat and freshwater fossils
Northern flank			
III_1	Section 4.5	Terrestrial (floodplain facies, basement)	Stiff clay
	Section 4.10	Barrier–lagoon	Sandy clay with sand lenses
	Section 4.11	Tidal sand ridge	Silty sand with clay
	Section 4.8	Tidal flat	Clayey silt and clayey sand
III_2	Section 4.9	Lacustrine	Mud with peat and freshwater fossils

counted for less than 10% of the sediment. Mud gravel was found in some cores. This facies is characterized by a fining-upward succession with an erosional surface at the bottom. No marine fossils or tidal sedimentary structures were found. The river channel environment was interpreted on the basis of the bottom erosional surface, the fining-upward succession, and the lack of marine fossils. The thickness of this facies ranges from 12 to 31 m, with an average of 19.3 m (Li et al., 2000).

4.2. Floodplain–estuary facies

This facies is composed of gray sandy clay. Sand lens, plant debris, and peat layers were often found in the lower part of the facies. A typical decreasing upward resistivity was logged in some of the cores. A few marine fossils were found, and where present, they exhibited indications of being transported (Li and Wang, 1998). In the upper part of the facies, tidal laminae and reactivation surfaces were well developed. In some cores at the present river mouth area, tidal laminae were developed in the entire section of the facies. The sedimentary environment of this facies was interpreted as floodplain–estuary based on its gradational contact with the underlying channel sand and the occurrence of well-developed tidal laminae. The thickness of this facies ranges from 10 to 30 m. The ^{14}C dating ranges from 9 to 14 ky BP (Table 2).

4.3. Estuary–prodelta facies

This facies is composed mainly of dark gray soft mud with thin silty laminae. The silty laminae are typically 1–2 mm thick, while the muddy laminae between them range from several cm to tens of cm.

Table 2
^{14}C dating in the floodplain–estuary facies overlying the channel-fill sand

Core ID	Depth (m)	^{14}C date years BP	Sample type	Reference
T16	32.9	9100 ± 110	Peat	This study
T16	34.4	9920 ± 110	Peat	This study
T16	48.4	12,000 ± 170	Organic mud	This study
T16	52.5	12,790 ± 310	Organic mud	This study
T16	54.6	14,640 ± 640	Organic mud	This study
C38	60.1	10,700 ± 125	Organic mud	Qin et al. (1987)
C4	54.7	12,630 ± 320	Peat	Qin et al. (1987)
T17	35.5	9900 ± 300	Organic mud	This study
T17	38.8	11,030 ± 123	Organic mud	This study

Core locations are shown in Fig. 1.

Vertical borrows were occasionally found. This facies is rich in foraminifers. The foraminifer assemblage, *Epistominella naraensis–Globigelinads–Elphidium magellanicum*, is typically interpreted as estuary–prodelta environment (Wang, 1985; Li and Wang, 1998). The thickness of this facies ranges from 2.0 to 24.5 m, with an average of 11.4 m (Li et al., 2000). The ^{14}C dating ranges from 4 to 8 ky BP (Li and Wang, 1998).

4.4. Deltaic facies

The deltaic facies comprises mouth-bar and distributary subfacies with a river mouth foraminifer assemblage (Li and Wang, 1998). The mouth-bar subfacies is composed of fine sand with thin muddy laminae and demonstrates a typical coarsening-upward succession. Sedimentary structures include cross-bedding, bi-directional cross-bedding, and planar bedding, indicating influences of tidal currents. Regionally, this facies appears as large sand lens, 10–15 km long and 10–30 m thick. The distributary subfacies is composed primarily of gray to yellowish gray clayey sand to sandy clay with an apparent fining-upward succession. An erosional surface, as indicated by a sharp contact, was often observed at the bottom. Tidal-related bi-directional sedimentary structures are common. Laterally, this facies is usually distributed along the sides of a river mouth bar.

4.5. Terrestrial stiff mud

The regionally distributed stiff mud is generally composed of 40–45% clay, 40–60% silt, and less than 5% sand. Plant roots and debris, and phytoliths occur in the upper portion. Vertical cracks are common. Micromorphologic analyses indicate typical soil characteristics, such as algillan, desiccation cracks, pedogenetic voids, plant roots and debris, and ferrugeneous and manganous nodules (Li and Sun, 1991; Li et al., 1995, 1996; Chen and Li, 1997; Deng et al., 1999). These features indicate that the stiff mud layer has been exposed extensively and has experienced pedogenesis. Based on the above characteristics, this regionally distributed stiff mud was interpreted as paleosol. Foraminifers, most of which are small, broken, and oxidized, were found in most of the analyzed cores, indicating that the foraminifers have been transported, possibly by storm surge or wind. Generally, fewer than five foraminifers were found in 50 g of dry samples. The lithology and abundant plant debris indicate terrestrial depositional environment, most likely floodplain (Liu, 1993; Chen, 1997). The ^{14}C dating of this layer ranges from 15 to 35 ky BP (Table 3). Compared to the other facies, this layer is easily distinguished due to its stiffness and abrupt contact with overlaying strata.

4.6. Marsh–nearshore facies

This facies is characterized by gray mud with 40–60% silt, 40–45% clay, and less than 5% sand. The lower portion contains abundant plant roots and debris with peat layers of up to several tens of cm. This portion was interpreted as coastal marsh due to its severe bioturbation, absence of sedimentary structures, abundant plant debris, and existence of peat layers. The upper portion of this facies contains a fair number of foraminifers, while the occurrence of plant debris is

Table 3
^{14}C dating at the top of the terrestrial stiff mud

Core ID	Depth (m)	^{14}C date years BP	Sample type	Reference
T28	28.30–28.50	14,196 ± 220	Organic mud	This study
T28	30.18–30.35	18,520 ± 520	Organic mud	This study
T5	23.50–23.80	15,005 ± 625	Organic mud	This study
C103	24.0	14,750 ± 150	Organic mud	Wu and Liu (1989)
C128	2.37	15,885 ± 170	Organic mud	Chang (1996)
T13	19.64–19.84	14,830 ± 390	Organic mud	This study
C150	33.3	>35,000	Shell	Wang et al. (1998)

Core locations are shown in Fig. 1.

rare. The upper portion was interpreted as nearshore environment (Wang, 1985; Li and Wang, 1998). The general absence of wave- and/or tide-induced sedimentary structures might indicate a rapid deposition of mud, probably caused by abundant sediment supply. The ^{14}C dating ranges from 8 to 12 ky BP (Li and Wang, 1998).

4.7. Shallow marine facies

This mud facies is characterized by a high water content of up to 70%, resulting in apparent softness. The dark gray soft mud contains 35–50% clay, 40–60% silt, and 3–5% sand. Thin sandy silt laminations were found in most cores. In addition to its softness, another distinctive characteristic of this facies is its high content of foraminifers, up to several-hundred individuals in 50 g of dry sample. The foraminifer assemblage, *E. naraensis–Ammonia beccarii* vars, is usually interpreted as shallow marine environment. This facies represents the maximum flooding in the Yangtze delta area (Wang, 1985; Li and Wang, 1998). Contacts with overlying and underlying strata are gradual.

4.8. Tidal flat facies

This facies is generally gray to yellowish gray mud and muddy sand with 30–60% fine sand, 20–50% silt, and 10–20% clay. A fining-upward trend is typical of this facies. Higher clay content was generally measured in the southern flank, while higher silt and sand contents were measured in the northern flank. Iron and manganese nodules and plant debris are common near the top of this facies. A sequence of sedimentary structures, including cross-bedding and flaser bedding in the lower portion, lenticular and wavy bedding in the middle, and horizontal bedding toward the top, was often identified. The combination of sedimentary structures indicates a tidal flat depositional environment, similar to those described by Reineck and Singh (1980).

4.9. Lacustrine facies

This facies is composed of gray mud containing freshwater algae, phytolith, and calcareous- or ferro-concretions. As many as three to four peat layers were found in some ores. This facies is characteristic of abundant plant roots and organic debris. Horizontal bedding and ripple marks, well developed in some cores, were observed, indicating the influence of currents. Mud layers, 10–20 cm thick, with whole oyster and brackish water shells occur in some cores, indicating local saltwater influence from tides. This facies was interpreted as freshwater-dominated lacustrine–marsh environment with local, limited tide influences (Li and Wang, 1998). The facies typically lies above the regional stiff mud, separated by a sharp contact.

4.10. Barrier–lagoon facies

This facies is composed largely of gray sandy mud with generally 20–30% sand, 20–40% silt, and 20–40% clay. Large sand lenses of 2–3 m thick were identified when correlating neighboring cores. Low-angle cross-bedding and mixtures of marine, brackish, and fresh water mollusk shells are common in the sand layers. The shells in the sand layers were typically broken, indicating a relatively high-energy coastal environment. The sand lenses were therefore interpreted as barrier island deposits. The adjacent mud deposits are rich in plant debris with occasional peat layers, indicating a back-barrier environment. The entire facies is interpreted as a transgressive barrier–lagoon system (Li and Wang, 1991).

4.11. Tidal sand ridge facies

This facies is of gray color with 40–80% sand, 15–40% silt, and 5–15% clay. Bi-directional cross-bedding and graded bedding are common in this sandy layer. The graded bedding is typically 10–20 cm thick and often superimposed forming rhythmics. Mollusk and foraminifer shells, both whole and broken, are common, indicating a relatively high-energy marine environment. The foraminifer assemblage, *E. naraensis–A. convexidorsa*, represents a typical shallow marine environment. An erosional surface was often observed at the bottom of this facies. The paleocurrents, obtained in the cores using environmental magnetic method, were bi-directional (Zhang et al., 1998), indicating apparent influence of tidal currents. This facies was interpreted as subaqueous tidal sand ridge (Li et al., 1999). The ^{14}C dating at the middle to lower portions of this facies indicates a time of deposition of 4–6 ky BP (Wang, 1993; Wang et al., 1997), after the maximum transgression at approximately 7 ky

BP (Ren, 1986). The ^{14}C dating below the bottom erosional surface is typically more than 10,000 ky BP, which suggests that the erosional surface represents a sedimentary hiatus of several thousand years.

5. Stratigraphic framework

The stratigraphic framework was established based on the vertical and horizontal distribution of the individual facies described above. For the convenience of description, four types of vertical facies-assemblage pattern were classified. Six transects, three longitudinal (roughly parallel to the coastline) and three latitudinal (perpendicular to the coastline), were examined (Fig. 1). Due to the nearly east–west dip of the delta, the longitudinal transect is roughly perpendicular to the axis of the delta, and the latitudinal is parallel to the delta axis.

5.1. Vertical facies assemblage

Four vertical facies patterns, referred to as types 1 through 4, were distinguished. The four types of facies assemblage reflect the stratigraphic characteristics induced by the transgression and regression in different regions of the delta.

Type 1 facies assemblage was generally found on the southern flank (II_1), primarily seaward of the postglacial transgression maximum (Fig. 3). A typical example of a type 1 facies assemblage is demonstrated in core T23 (Fig. 5). The base layer of type 1 facies

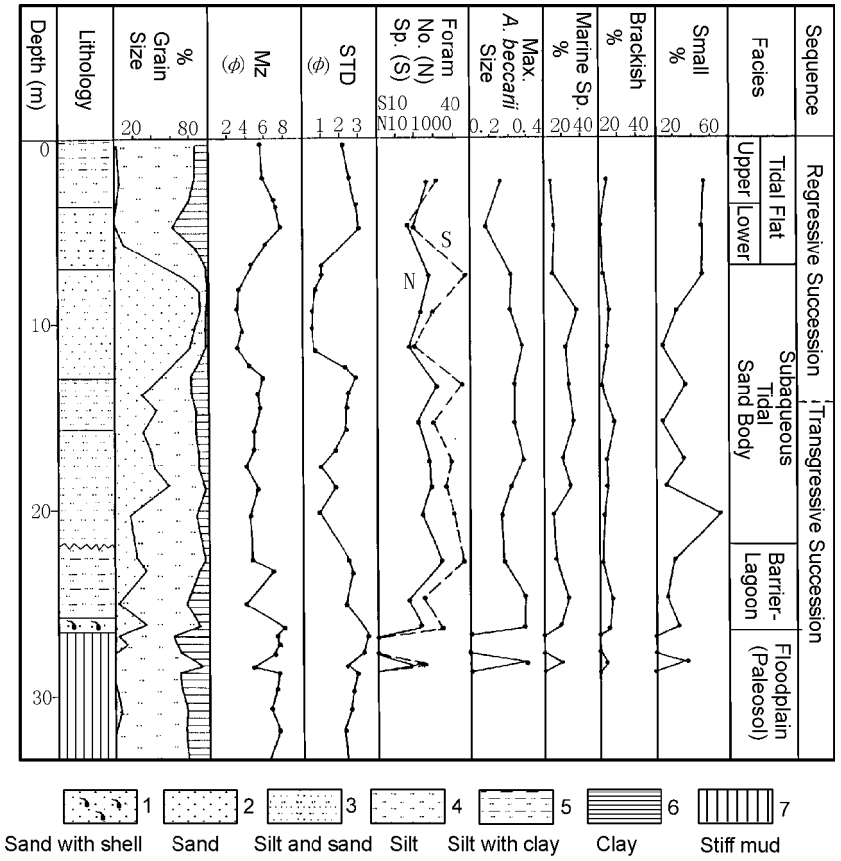

Fig. 6. Type 2 facies assemblage illustrated by core T8.

assemblage is the distinctive terrestrial stiff mud. Three facies overlie the stiff mud, including, from bottom to top, marsh–nearshore facies, shallow marine facies, and tidal flat facies. Maximum transgression was reached during the deposition of the shallow marine soft mud and the maximum flooding surface is located in the soft mud layer, below and above which, transgressive and regressive successions were developed, respectively.

Type 2 facies assemblage was generally found on the northern flank (III_2), primarily seaward of the post-glacial transgression maximum. A typical example of type 2 facies assemblage is illustrated in core T8 (Fig. 6). Overlying the terrestrial stiff mud base layer, barrier–lagoon facies, tidal sand ridge facies, and tidal flat facies occur upward. An apparent erosional surface was often found at the bottom of the tidal sand. The erosional surface represents the maximum flooding surface and was therefore considered to be the boundary separating the transgressive and regressive successions.

Type 3 facies assemblage was generally found landward of the post-glacial transgression maximum (II_2, III_2), but the marine influence can still be identified (Fig. 7). The thickness of the type 3 facies assemblage typically ranges from 3 to 12 m. The lacustrine facies was identified overlying the terrestrial stiff mud. The ^{14}C dating at the bottom of the lacustrine facies ranges from 5 to 6 ky BP (Li and Wang, 1998).

Type 4 facies assemblage was generally found in the delta main body (I). This facies assemblage demonstrates a characteristic decreasing upward resistivity log (Fig. 8). An example of the type 4 facies assemblage is illustrated in core T16 (Fig. 9). A distinctive erosional surface lies at the bottom of this facies assemblage. From bottom to top, the type 4 assemblage typically includes river channel facies, floodplain–estuary facies, estuary–prodelta facies, and tidal flat facies. The post-glacial transgression maximum was reached during the deposition of the estuary–prodelta soft mud. In some cores, e.g., T16, the estuary–prodelta soft mud was eroded by the distributary channel, and the erosional surface serves as the boundary separating the transgressive succession beneath and the regressive succession above (Fig. 9). Type 4 facies assemblage represents the post-glacial sequence of incised-valley fill.

5.2. Stratigraphic framework

Three longitudinal and three latitudinal cross-sections were examined to depict the stratigraphic framework of the Late Quaternary Yangtze delta (Fig. 1). The seaward-most longitudinal cross-section B–B′, composed of 18 cores, cuts across the modern river

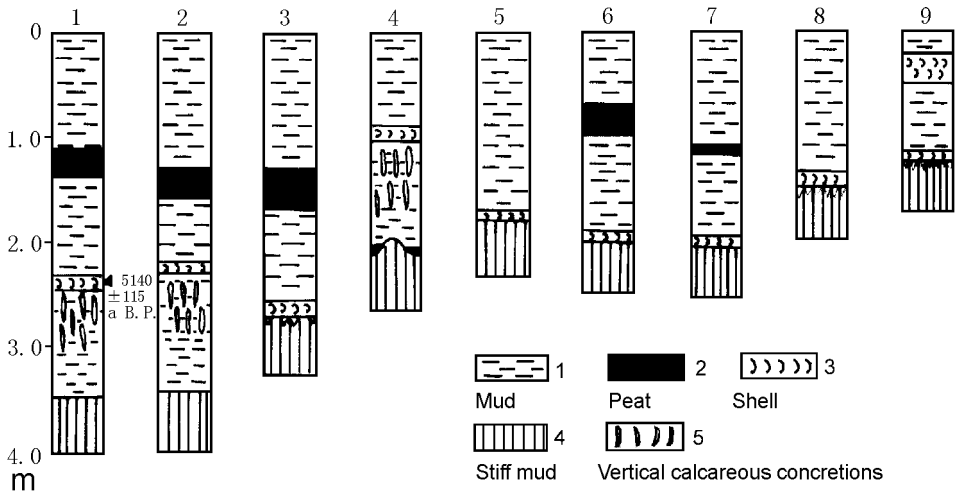

Fig. 7. Type 3 facies assemblage illustrated by a series of trenches in the vicinity of core T2.

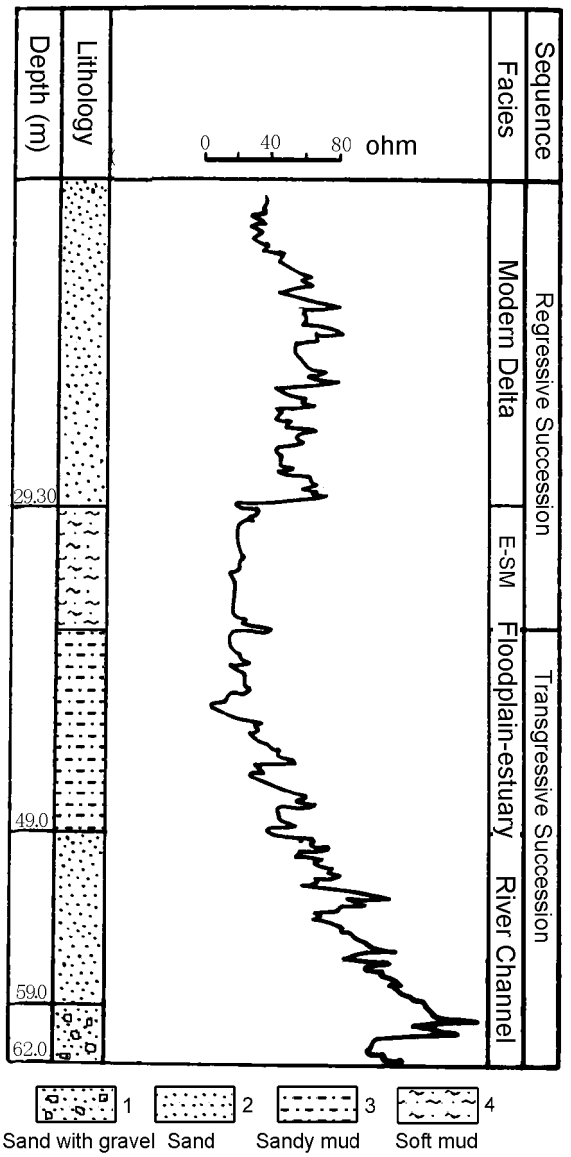

Fig. 8. Resistivity log of core C20, demonstrating the decreasing-upward floodplain–estuary facies. E-SM: Estuary–shallow marine facies.

mouth area. Eight cores were located on the delta main body. These relatively deep cores have an apparent erosional surface at the bottom, overlying which type 4 facies assemblage (incised-valley fill) was identified (Fig. 10). The terrestrial stiff mud layer underlies the cores on the two flanks. The four cores on the southern flank were composed of type 1 facies assemblage. The six cores on the northern flank demonstrated typical type 2 facies assemblage. The erosional surface at the bottom of the middle eight cores and the paleosol (stiff mud) in the cores on the flanks constitute the regional sequence boundary, on top of which the post-glacial sedimentary cycle developed. The sequence boundary (erosional surface) in the middle eight cores is substantially deeper than that (paleosol) in the cores on the flanks. This demonstrates a paleo-morphology with an incised valley in the middle and interfluve on the two flanks. The post-glacial transgression maximum was reached during the deposition of the estuary–prodelta facies in the middle cores and the shallow marine soft mud in the cores on the southern flank. While on the northern flank, evidence of a transgression maximum was largely erased by the erosional surface at the bottom of the tidal sand ridges. The post-glacial transgression maximum was dated at 7.5 ky BP in the estuary–prodelta facies in the incised-valley, slightly older than the 5–7 ky BP dated in the shallow marine soft mud on the southern flank (Liu et al., 1985; Ren, 1986; Li and Wang, 1998).

The shore-parallel section C–C′ is located landward of B–B′. Type 4 facies assemblage (incised-valley fill) was identified in the middle four cores (Fig. 11). The thickness and the characteristics of the incised-valley fill succession are comparable to that along section B–B′. However, the interfluvial sequence identified on the two flanks is thinner than that along section B–B′, ranging from 3 to 12 m thick. Type 3 facies assemblage dominated on both the northern and southern flanks.

The third shore-parallel section D–D′ is located further landward. Similar to sections B–B′ and C–C′, the incised-valley fill sequence (type 4 facies assemblage) was found in the middle cores and interfluvial sequence with type 3 facies assemblage identified on the two flanks (Fig. 12). The interfluvial sequence is even thinner than that along transect C–C′, ranging from only 1 to 2 m thick.

The first latitudinal (shore-perpendicular) section, A–A′, cut through the middle of the modern delta. The lower boundary of the post-glacial depositional cycle characterized by the type 4 facies assemblage is an erosional surface, which was found in all the deep cores. The thickness of the incised-valley fill sequence

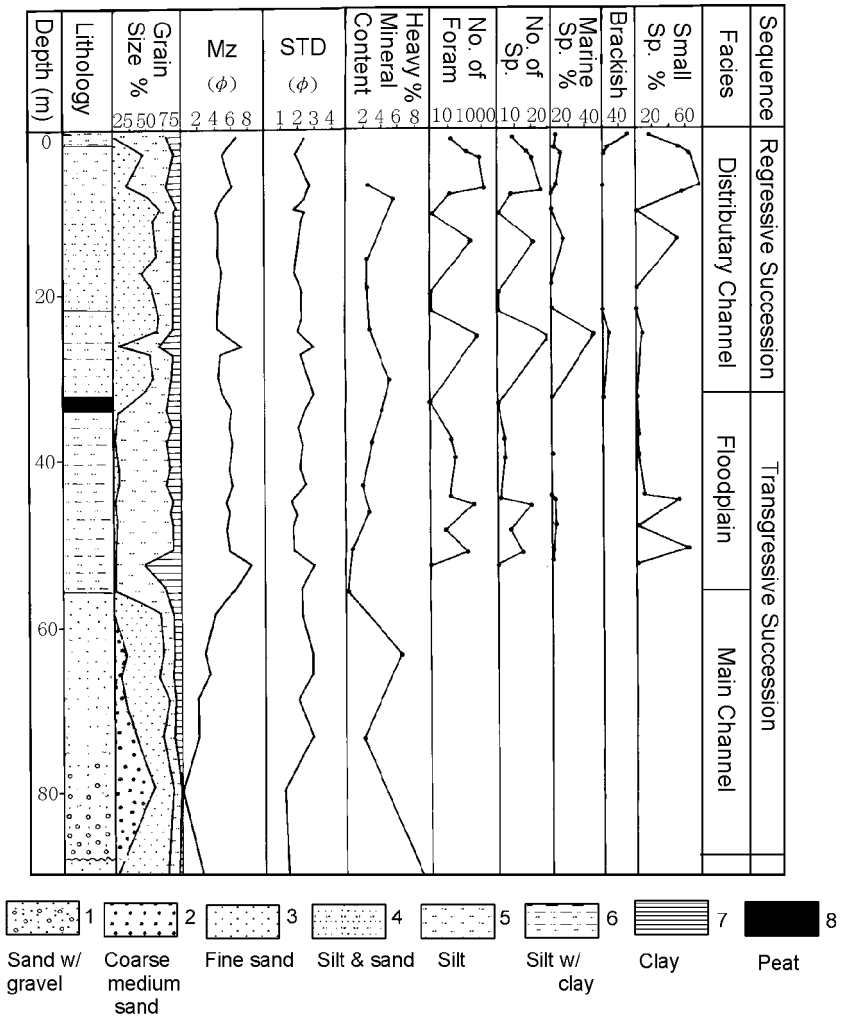

Fig. 9. Type 4 facies assemblage illustrated by core T16.

tends to increase seaward (Fig. 13). The post-glacial transgression maximum was reached during the deposition of the estuary–prodelta mud in most of the cores, while toward the apical area of the delta, the stratigraphic record was erased by an erosional surface. Beneath the maximum flooding surface, a transgressive succession consisting of, from bottom to top, river channel facies, floodplain–estuary facies and a portion of the estuary–prodelta facies, was identified. Above the maximum flooding surface, a regressive succession consisting of a portion of the estuary–prodelta facies, deltaic facies, and tidal flat facies was developed. The thickness of the transgressive succession is on average approximately 54% of the total thickness of the post-glacial depositional cycle (Li et al., 2000).

Cross-section E–E′ extends approximately parallel to the Yangtze River across the southern flank of the delta. The terrestrial stiff mud (paleosol) marks the lower boundary of the post-glacial depositional cycle (Fig. 14). The post-glacial transgression maximum was reached during the deposition of the shallow marine facies. The thickness of the shallow marine facies decreases landward and pinches out. The marine-influenced facies was replaced by lacustrine

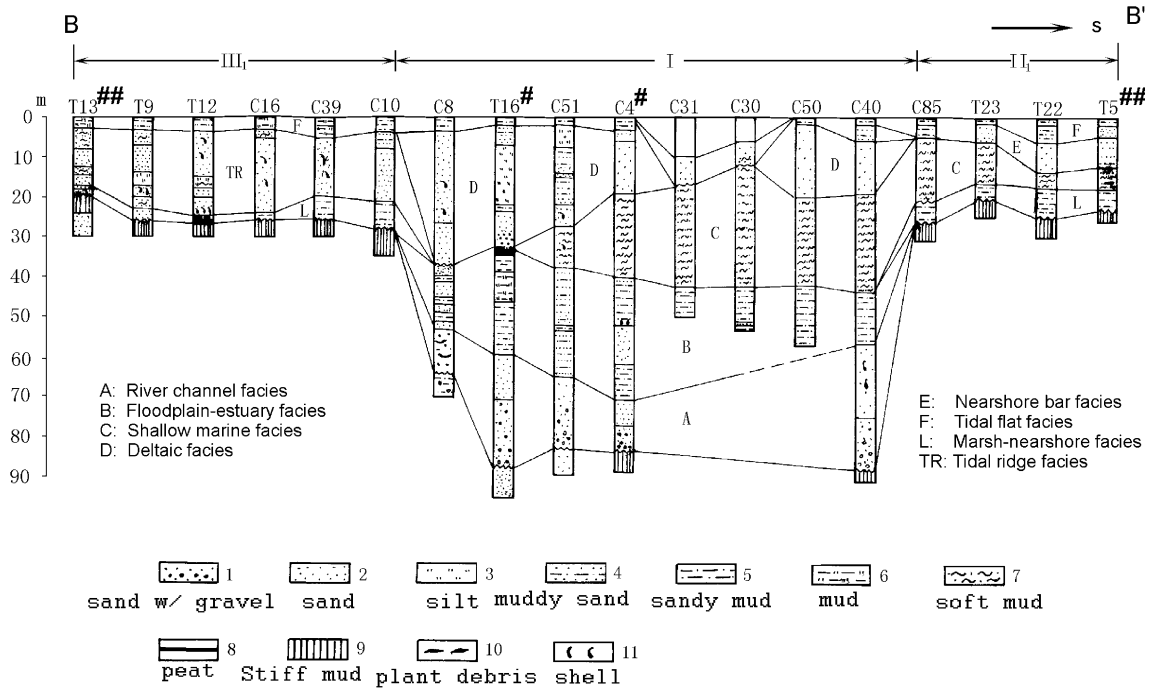

Fig. 10. Cross-section B–B′. I: Main delta (incised valley); II_1: southern flank seaward of the maximum transgression (paleo-interfluve); III_1: northern flank seaward of the maximum transgression (paleo-interfluve). #: See Table 2 for ^{14}C dates; ##: see Table 3 for ^{14}C dates.

facies landward of the post-glacial transgression maximum (Fig. 14). The thickness of the post-glacial cycle decreases landward from nearly 25 m in the vicinity of the present shoreline to less than 3 m in the Taihu Lake area.

Similar to E–E′, cross-section F–F′ on the northern flank of the delta demonstrates a landward-decreasing trend of the post-glacial strata thickness, indicated by the decreasing burial depth of the lower boundary (paleosol). Two distinctive differences were identified when comparing the stratigraphy of the northern and the southern flanks (Figs. 14 and 15). Firstly, the sediment is generally coarser, dominated by sandy deposits on the northern flank, as compared to that on the mud-dominated southern flank. Secondly, on the northern flank, the evidence of transgression maximum was usually erased by the strong tidal currents, leaving an erosional surface as an indicator of the maximum flooding (Zhao et al., 1997; Li et al., 1999). The tidal ridge facies overlying the erosional surface was deposited during the Holocene regression.

6. Origin and fill of the incised-valley system

The cross-sections discussed above revealed an incised-valley system in the Yangtze delta area. The incised valley is approximately 60–100 m deep and 60–70 km wide near the river mouth, and decreases to 20–30 km wide toward the delta apex. The incised-valley extends roughly 250 km across the studied area. Paleosol, as represented by the terrestrial stiff mud, is distributed broadly along the valley banks. In areas with dense core coverage, e.g., in Shanghai and Haian areas, secondary incised valleys representing tributaries can be identified (Fig. 16). The Yangtze incised-valley system is therefore composed of the main valley, the interfluve, and the tributary channels (Fig. 16).

6.1. Origin of the incised-valley system

Although incised valleys may be formed under the combined controls of tectonic uplift and sea-level fall (Fisk and McFarlan, 1955; Dalrymple et al., 1994;

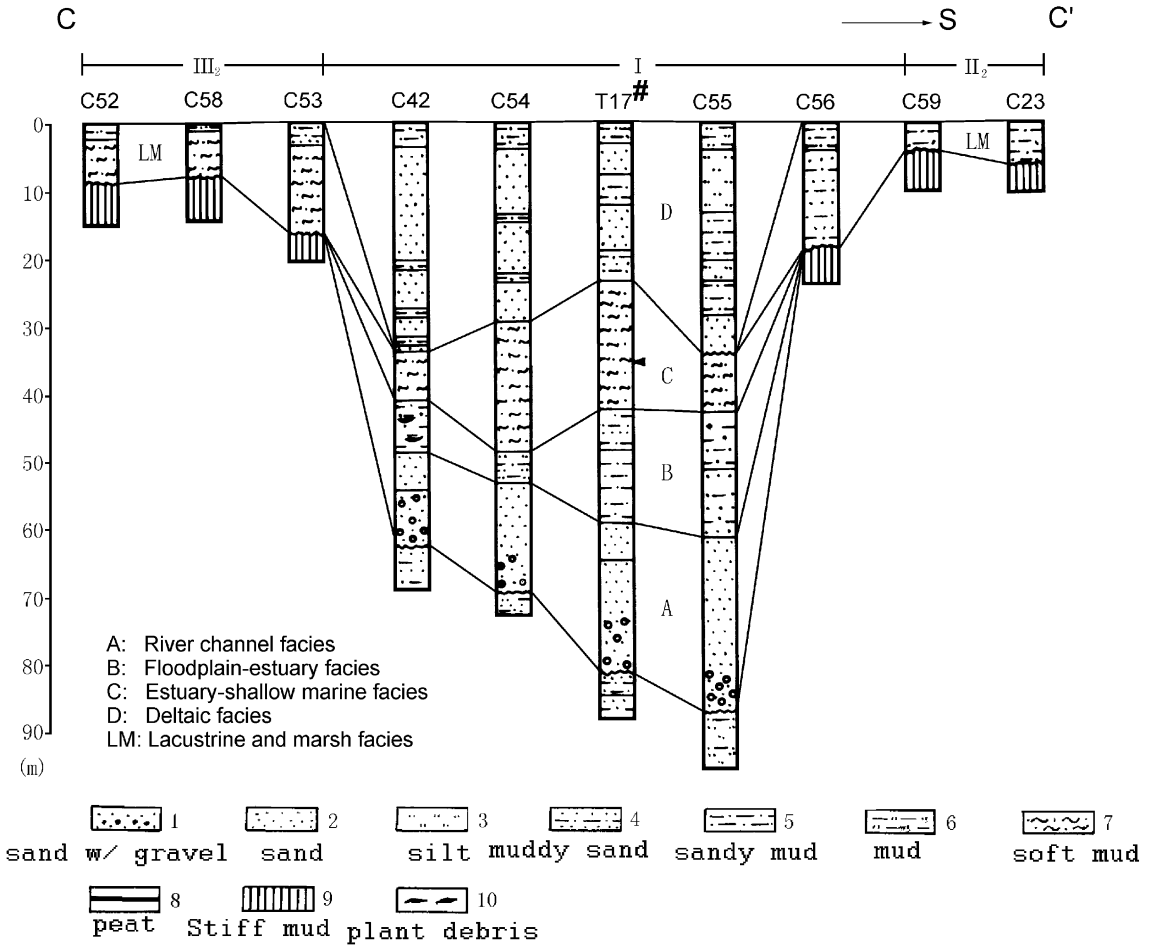

Fig. 11. Cross-section C–C′. I: Incised valley; II_2: southern flank landward of the maximum transgression; III_2: northern flank landward of maximum transgression. #: See Table 2 for ^{14}C dates.

Gupta, 1997, 1999), the Yangtze valley was incised largely due to sea-level fall, probably rapid fall, because it is located in a tectonic subsidence zone. The incision likely originated during the falling sea level during the $\delta^{18}O$ stage 3 (Martinson et al., 1987). During the latest glacial maximum, sea level fell approximately 130 m below the present level (Zhu et al., 1979). The great hydraulic drop and tremendous water discharge of the Yangtze River were the driving forces for the 60–100 m valley incision in the study area. Rapid valley incision probably occurred during the fast sea-level fall through $\delta^{18}O$ stage 3 (Fig. 17, period A). During the early part of $\delta^{18}O$ stage 2 (sea level at low stand), the valley incision continued (Fig. 17, period B_1), although possibly at a slower rate, as a result of the slower rate of sea-level fall approaching the pivot point. Normally, coarse lag deposits are found at the bottom of 'incised valleys' (Zailin et al., 1994); however, no layered lag deposits with significant thickness were identified in the study area, although gravel grains (typically less than 10%) were identified in many cores. In other words, lag deposition was not significant in the study area, and when it occurred, it was treated as part of the transgressive succession (Li and Wang, 1998; Li et al., 2000).

6.2. Fill of the incised-valley system

Since the studied Yangtze valley is located in a tectonic subsidence zone, the valley fill probably

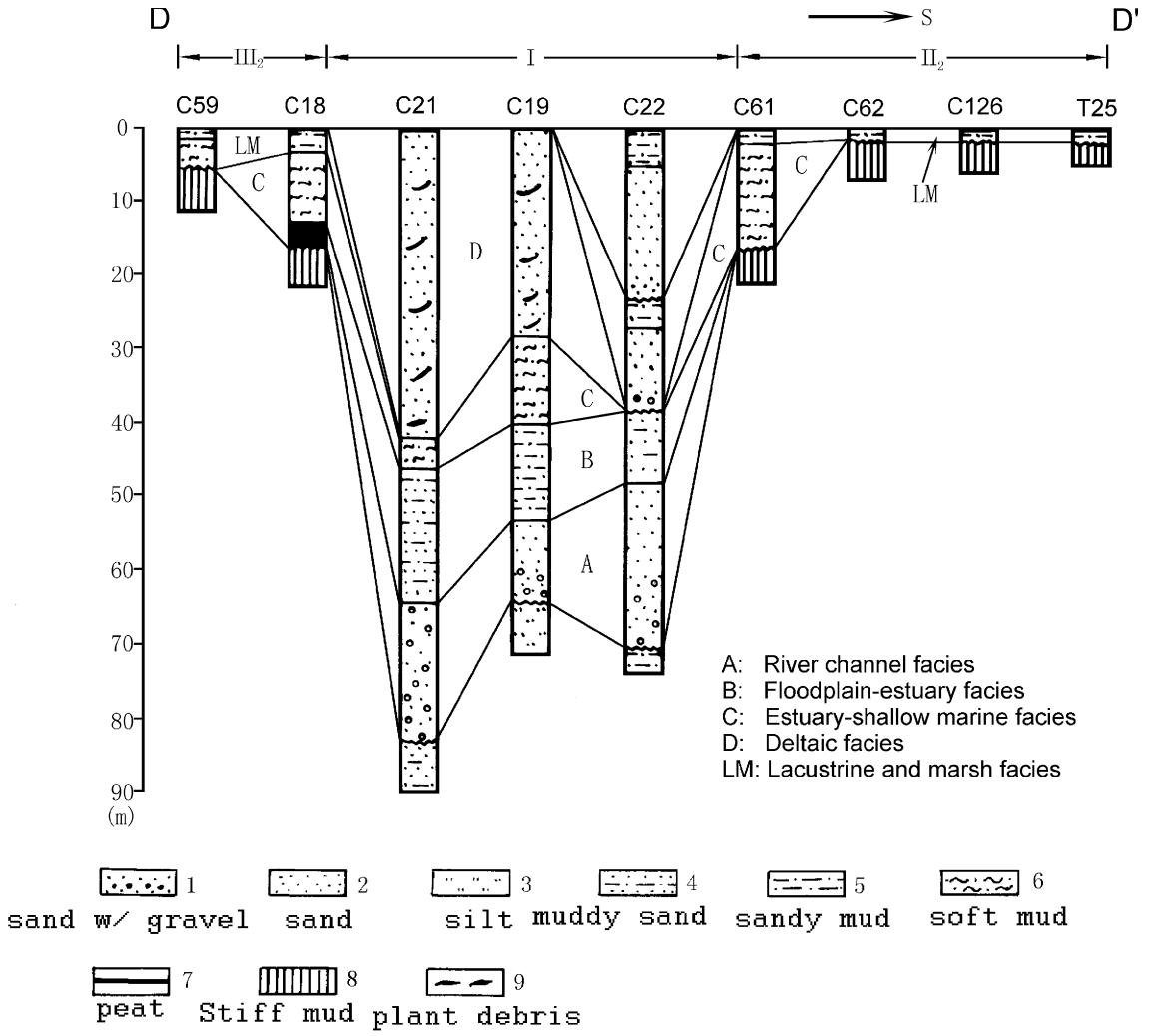

Fig. 12. Cross-section D–D′. I: Incised valley; II_2: southern flank landward of maximum transgression; III_2: northern flank landward of maximum transgression.

originated when the sea-level fall ceased. The post-glacial transgression-induced valley fill can be subdivided into two stages. The early stage is characterized by incised-valley fill without the direct influence of tidal currents (Fig. 17, period B_2), while the late stage is characterized by estuary formation with strong influence from tidal currents (Fig. 17, period C_1).

6.2.1. Early stage of transgression and deposition of the channel sand

The incised-valley channel sand facies, which was deposited immediately on top of the sequence boundary, is generally 20–30 m thick, or roughly 20–35% of the total thickness of the post-glacial depositional cycle (Li et al., 2000). No marine microfossils and tidal sedimentary structures were found in the channel sand facies. The general lack of marine fossils and tidal sedimentary structures was explained by the process of retrogressive aggradation coping with the post-glacial sea-level rise. Sediment aggradation induced by base-level rise has been described and studied by river and water-reservoir engineers for decades (e.g., Gessler, 1971; Simons and Senturk, 1977; Qian et al., 1989). Aggradation induced by

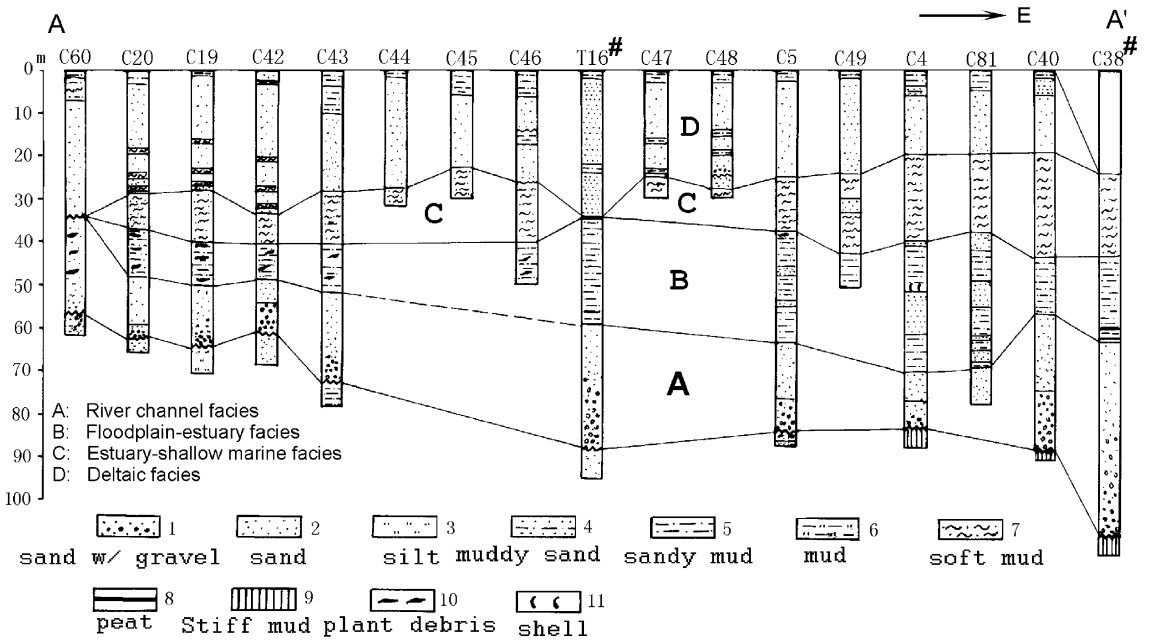

Fig. 13. Section A–A′ across the delta main body. #: See Table 2 for ^{14}C dates.

construction of reservoirs and associated river dams has been measured a considerable distance upstream (Borland, 1971). The highest elevation influenced by the aggradation can be substantially higher, e.g., tens of meters, than the maximum water level in the reservoir (Qian et al., 1989). The aggradation was in-

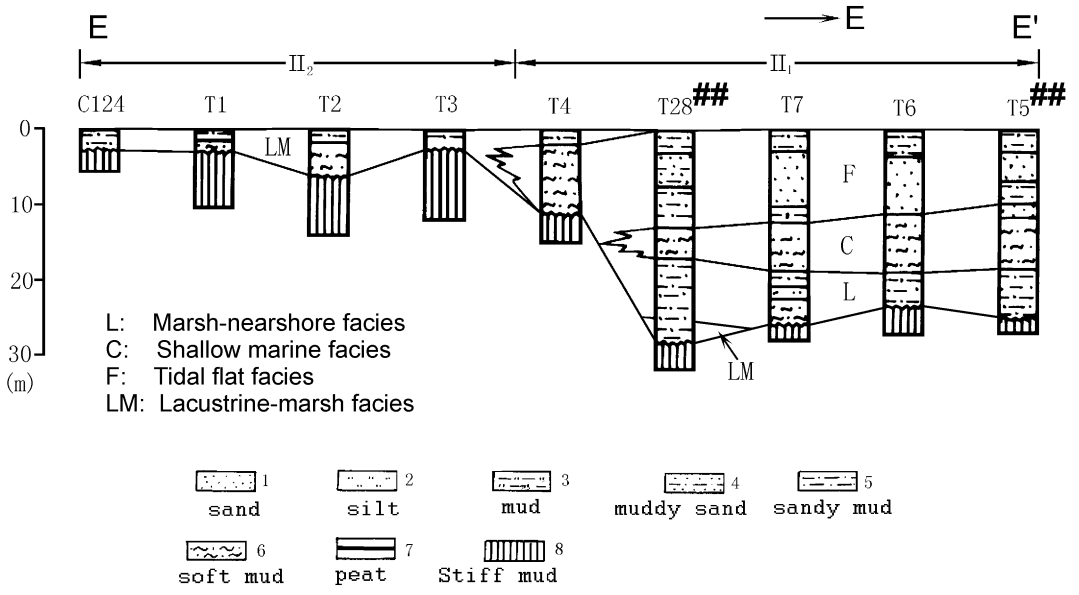

Fig. 14. Section E–E′across the southern flank of the delta. II_1, II_2: Seaward and landward of maximum transgression, respectively. ##: See Table 3 for ^{14}C dates.

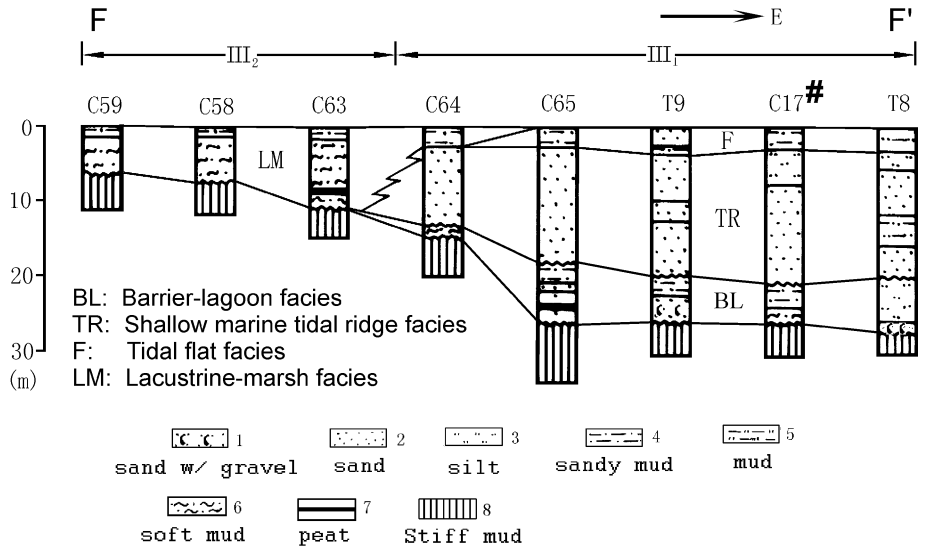

Fig. 15. Section F–F′ across the northern flank. III_1, III_2: Seaward and landward of maximum transgression, respectively. #: See Table 2 for ^{14}C dates.

terpreted as the result of equilibrium-profile justification corresponding to the rise of the base level (Gessler, 1971). As described in Posamentier and Vail (1988), base-level rise creates new accommodation space. Given the abundant sediment supply, as the equilibrium profile adjusts relative to the new base level and the river mouth shifts landward, upstream accumulation occurs. A continuous rise of base level, therefore, results in a continuous onlap succession of aggradation. Variations of the sea-level rise rate and sediment supply may complicate the process of retrogressive aggradation. The fining-upward succession and the absence of marine fossils, as observed in the Yangtze incised-valley fill, are the results of retrogressive aggradation (Li, 1984, 1986; Li et al., 1988, 2000).

During the spring tide in the dry season, the flood tidal current was measured in the vicinity of Yangzhong area (Fig. 1), approximately 230 km upstream from the present river mouth (Li et al., 1983). Foraminifers were found upstream at similar distance (Li et al., 1983; Cheng, 1987). The foraminifers found in the surface sediment landward of the river mouth were all dead, with an upstream decreasing trend in number and size (Li et al., 1983; Cheng, 1987). This indicates that the foraminifers were likely transported by the flood tidal current to approximately 230 km upstream from the present river mouth.

The fact that marine microfossils are absent from the fining-upward channel-sand facies indicates that the location of its deposition should be further landward of the upper limit of direct flood tidal current influence, as discussed in the previous paragraph. In other words, the landward extent of the retrogressive aggradation caused by the sea-level rise was beyond the limit of direct tidal current influence, as indicated by the presence of transported marine fossils and tidal sedimentary structures. Although marine fossils were not found in this facies, the deposition of this relatively thick sandy layer was a direct result of sea-level rise, and therefore, this facies was interpreted as part of a transgressive succession.

Makkaveev (1960) conducted flume experiments to examine the extent of backwater and retrogressive aggradation caused by base level rise, and found that the extent of retrogressive aggradation could reach beyond that of the backwater. The average water-surface gradient in the lower reach of the present Yangtze River is approximately $1:140 \times 10^3$. Therefore, the backwater induced by a 3-m rise of tide should extend roughly 420 km upstream from the river mouth. In other words, the extent of backwater

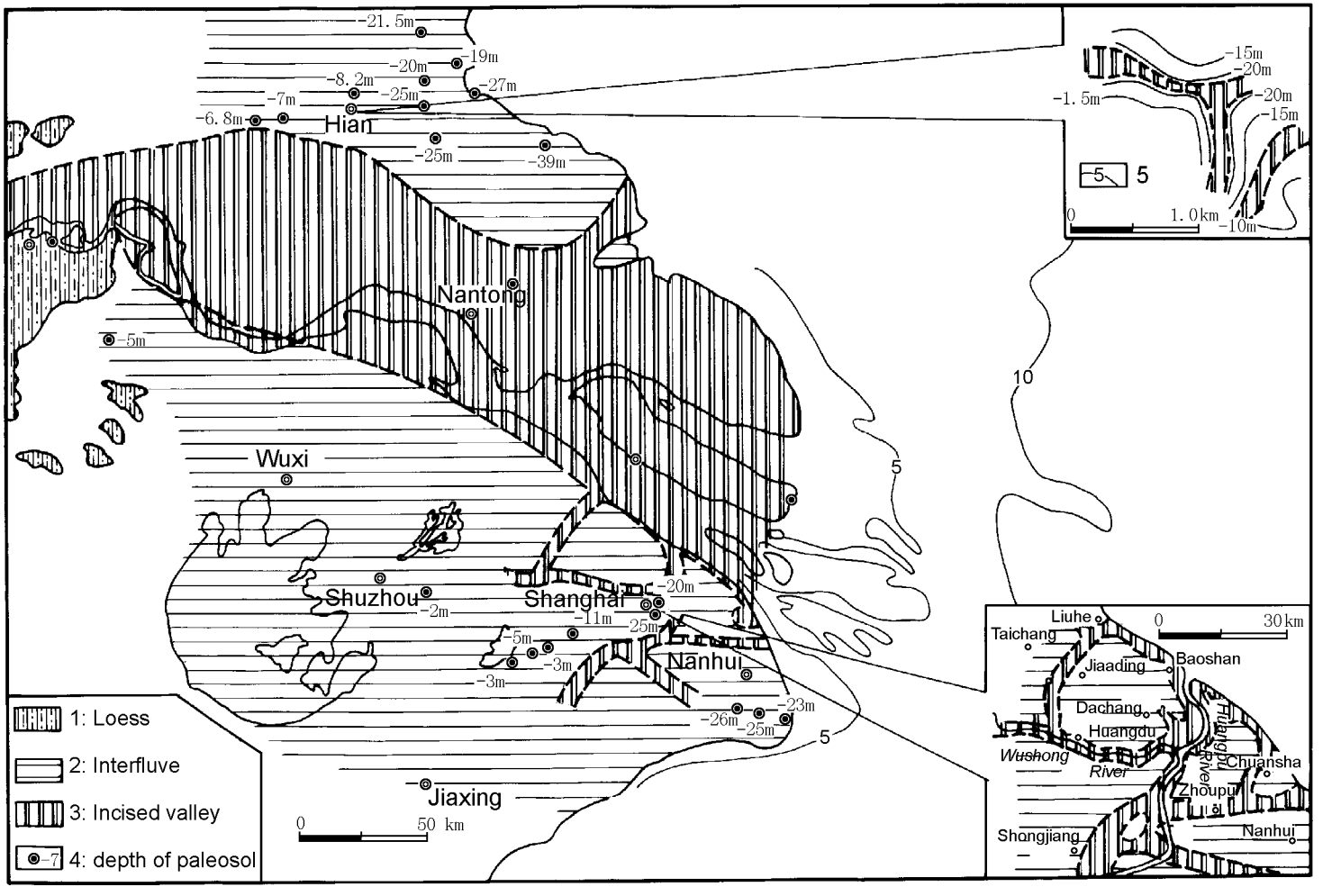

Fig. 16. The Yangtze incised valley system including main channel and distributaries valleys (insert figures, where dense core coverage or geophysical data are available).

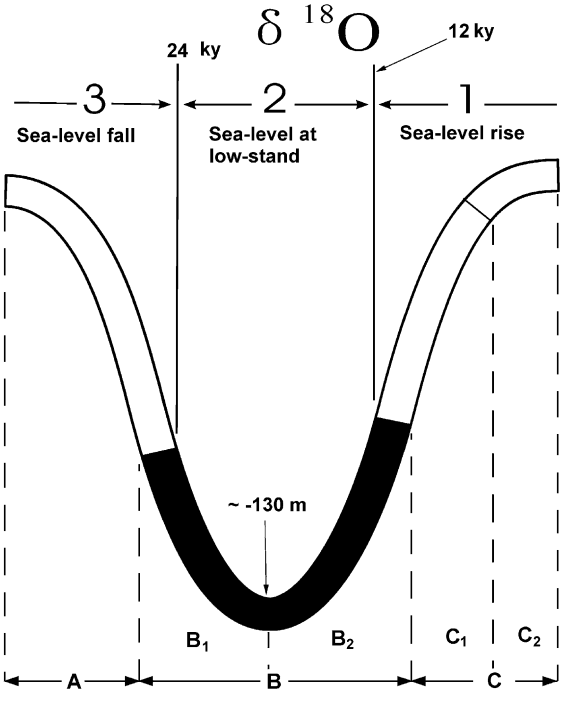

Fig. 17. Relationship of sea-level change and Yangtze incised valley formation and fill.

(420 km), which is shorter than that of retrogressive aggradation, is longer than the reach of the flood tidal current (230 km). This provides another piece of evidence that the present study area was at least 230 km landward of the paleo-coastline during the initial incised-valley fill in the study area. The backstepping aggradation process has also been used to interpret channel fill in rock records (Gupta, 1999).

6.2.2. Late stage of transgression and estuary formation

The boundary between the early and late stages of valley fill is likely gradual as indicated by the gradual transition between the channel-sand facies and the overlying floodplain–estuary facies. In other words, the boundary between periods B_2 and C_1 in Fig. 17 is probably gradual and not necessarily separated by the $\delta^{18}O$ stages.

Overlying the channel-sand facies, massive mud with peat layers, which is characteristic of floodplain deposits, was often identified. Due to limited core coverage, regional distribution of the floodplain deposits could not be correlated consistently, and it will therefore be discussed together as the floodplain–estuary facies, as it has been in the previous sections. As sea-level rise continued, the incised valley was inundated, and the development of an estuary started sometime during period C_1 in Fig. 17. The estuary widened and extended landward with continued sea-level rise, and finally achieved its maximum size with its apex reaching Zhenjiang–Yangzhou area during the post-glacial transgression maximum, at around 7.5 ky BP. The present, neighboring Qiantanjiang Estuary (Figs. 1 and 18) may provide a modern analog of this paleo-estuary (Li and Li, 1983; Li, 1984; Zhang and Li, 1996). With the development of the estuary, flood and ebb tidal currents became important factors, leading to the formation of tidal lamination and the redistribution of foraminifers. This floodplain–estuary facies with well-developed tidal laminae and transported foraminifers lies between the estuary–prodelta facies and channel-sand facies, and can reach a thickness of nearly 30 m in cores located near modern river mouth area. Marine influence is apparent due to the common occurrence of foraminifers and tidal sedimentary structures, although the foraminifers have shown evidence of being transported. Tidal currents are believed to be the main mechanism for the foraminifer transport.

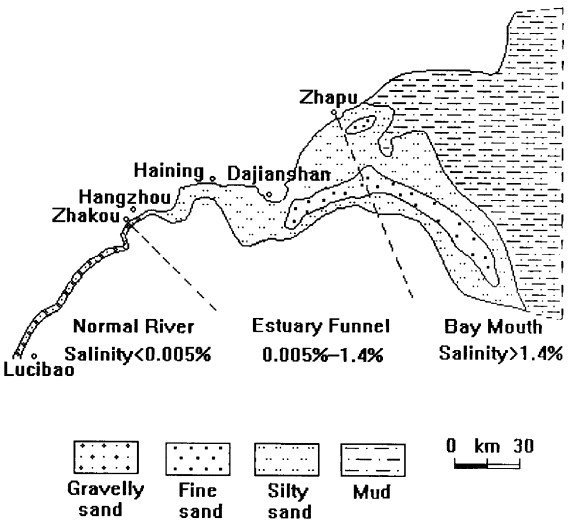

Fig. 18. Sediment distribution of the present Qiantangjiang Estuary, see Fig. 1 for general location (modified after Zhang and Li, 1996).

Coping with the continued sea-level rise, the coastline along the two flanks, i.e., the paleo-interfluve, retreated. Controlled by the incised-valley morphology, the water depth was significantly shallower on the two flanks than over the valley. On the northern flank, a wave-dominated environment, characterized by barrier–lagoon systems, developed, while on the southern flank, a tidal flat environment dominated. The substantial sedimentary difference between the northern and southern flanks can be attributed to the following factors: (1) the original slope was steeper on the northern flank and gentler on the southern flank, and (2) the southern flank tends to receive much more fine grain sediment than the northern flank.

6.3. Holocene regression and development of the Holocene delta

As the tremendous sediment supply overcame the slowing rate of sea-level rise during the late $\delta^{18}O$ stage 1 (Fig. 17, period C_2), regression started. Like many other deltas in the world (Stanley and Warne, 1998), the Holocene Yangtze delta developed in a regression environment. The regressive succession is generally thicker with coarser sediment at the apical area (e.g., Fig. 13, C60, C20, C19, and C42) than at the river mouth area. A bottom erosional surface was sometimes identified at the apical area. A large sand body, which is 2–3 m higher in elevation than the surrounding deltaic plain, was identified in the vicinity of the apical area (the sand body surrounding Hongqiao area in Fig. 2). This thick sand unit, with a relative high elevation and a bottom erosional surface, similar to that in modern Qiantanjiang Estuary (Qian et al., 1964; Zhang and Li, 1996), seems to indicate a greater hydrodynamic energy near the apical area than other areas in the estuary. Core-correlation in section A–A′ indicates that the sediments tend to become finer seaward, similar to that in the modern Qiantanjiang Estuary (Fig. 18). This seaward fining trend differs from the broadly accepted model including, from land to sea, coarser bay head-delta, finer central basin and coarser mouth-bar units (Roy, 1984, 1994; Allen and Posamentier, 1993; Dalrymple et al., 1994; Zaitlin et al., 1994; Roy et al., 1995; Nichol et al., 1996, 1997).

As mentioned above, the Yangtze paleo-estuary demonstrates many similarities to the modern Qiantanjiang Estuary. The trumpet-shaped Qiantanjiang Estuary has a tidal range of 5–6 m with a maximum of nearly 9 m at the apical area, much greater than the 2–3 m range in the mouth area. Tidal currents of up to 3.0–3.5 m/s were measured at the apical area, also much larger than the 0.5–1.0 m/s near the mouth (Qian et al., 1964; Zhang and Li, 1996). It is reasonable to deduce that the tidal ranges and tidal currents in the Yangtze paleo-estuary should be close to that in the modern Qiantanjiang Estuary. Existence of an ancient Yangtze tidal bore at the apical Zhenjiang area has been documented by Chen (1989). In other words, the ancient Yangtze estuary might have been macro-tidal, probably influenced by its trumpet shape. As the development of the Holocene delta continued with further regression, the influence of shape was reduced and the Yangtze estuary changed from macro-tidal to meso-tidal.

Six stages of sub-delta development have been identified, partially based on the evolution of the mouth bars (Fig. 2). The mouth-bar development began in the northwest and gradually migrated toward the southeast, with the southern distributary gradually becoming the main channel during each stage of sub-delta development (Li et al., 1979; Li and Li, 1983; Li, 1984). The distribution patterns of the sand bodies were discussed in detail in Li (1984, 1986) and are beyond the scope of this paper. The trend of the southward migration of the sand-body developments was also observed at the modern river mouth (Li et al., 1979; Li, 1986; Chen, 1998).

6.4. Evolution of the two flanks during the Holocene regression

The Yangtze delta initially developed within the bounds of the incised valley. As sea-level rise continued, deposition facilitated by the tremendous sediment supply began on the two banks started at around 5–6 ky BP. Depositions on the northern and southern flanks demonstrated quite different characteristics, probably controlled by different initial slope, riverine sediment redistribution, and tidal forcing. The northern flank is dominated by the development of tidal sand bodies (Li et al., 1999, 2001), while the southern flank was dominated by accumulation of finer tidal flat deposits. The southward transport of the fine sediment also provides the main sediment supply for

the huge silt-sand body in the neighboring Qiantanjiang Estuary (Qian et al., 1964; Zhang and Li, 1996).

Studies of paleo-tidal dynamics indicated that there was a convergent–divergent tidal current system on the northern flank during 5–6 ky BP, caused by the interaction between the progressive tidal wave from the Pacific Ocean and the reflected tidal wave from Shangdong Peninsula (Shen et al., 1993; Li et al., 2001). This convergent–divergent tidal system provided a favorable condition for the development of tidal sand ridges. As the regression continued, these tidal sand ridges became the main stratigraphic unit on the northern flank (Li et al., 1999, 2001). A radial tidal sand ridge system is currently developing in the offshore portion of the northern flank. The sand ridges identified in the cores probably reflect a future stage of the present offshore tidal sand ridges (Li et al., 1999, 2001), if the regression continues. The rate of coastline propagation on the northern flank was approximately 3–5 m/year from 5 to 1 ky BP and increased dramatically to 40–70 m/year since 1128 AD when the Yellow River debouched into the Yellow Sea in northern Jiangsu (Ren, 1986; Li and Zhang, 1997).

Seaward of the post-glacial transgression maximum on the southern flank, the regressive succession is predominately composed of muddy deposits. The sand bodies found in the cores tend to be parallel to the paleo-coastline and were interpreted as longshore bars (Li and Li, 1983). Three to five cheniers were identified along the line of the Holocene transgression maximum (Liu et al., 1985). The coastline propagated 4–8 km seaward from 6 to 3 ky BP, at a rate of 1–2 m/year. The rate of coastline propagation accelerated to 20–30 m/year since 3 ky BP, as a result of the slowing sea-level rise (Liu et al., 1985; Li and Zhang, 1997).

Landward of the post-glacial transgression maximum on both the northern and southern flanks, freshwater lacustrine deposits dominated with limited, localized marine influence. The overall thin strata resulted from the inadequate sediment supply from the river and the limited accommodation space. The underlying stiff mud (paleosol), the localized marine influence, and the similar ^{14}C dates of 5–6 ky BP provided some guidance for correlation of strata with the strata seaward of the transgression maximum. These areas were exposed during low stand of sea level and most of the post-glacial transgression, and were inundated by freshwater when the post-glacial transgression reaches its maximum. Some shallow river channels connected the otherwise terrestrial environment with the sea, the Yangtze, or the Qiantanjiang estuaries (Chang, 1996; Li and Wang, 1998). These channels are probably the origin of the localized marine influences identified in the cores.

7. Conclusion

The stratigraphic framework of the Late Quaternary Yangtze delta demonstrates a large-scale incised-valley fill system. The regional sequence boundary is composed of the erosional surface at the bottom of the incised valley and the paleosol in the interfluve along the two flanks. The Late Quaternary stratigraphic framework is composed of one transgressive succession overlying the regional sequence boundary and one regressive succession, which comprises most of the Holocene delta. The maximum flooding surface is located in the distinctive soft marine mud. On the northern flank, the maximum flooding surface was represented by an erosional surface that resulted from the strong tidal currents, with subsequent deposition of tidal sand ridges. The thickness of both transgressive and regressive successions decreases landward, with decreasing marine influence and increasing fluvial influence.

Two general paleo-morphological units existed during the post-glacial low stand of sea level: an incised valley and interfluve. The incised valley and interfluve coincide roughly with the Holocene delta main body and its two flanks, respectively. From bottom to top, the incised-valley fill sequence is typically composed of the river channel facies, floodplain–estuary facies, estuary–prodelta facies, and tidal flat facies. The interfluvial sequence on the southern flank is typically composed of, from bottom to top, marsh–nearshore facies, shallow marine facies, and tidal flat facies, indicating dominant tidal influence. The interfluvial sequence on the northern flank is typically composed of, from bottom to top, the barrier–lagoon facies, tidal sand ridge facies, and tidal flat facies, indicating combined influence of both tidal currents and waves. The northern flank is dominated by relatively sandy deposits, while the southern flank is dominated by relatively muddy deposits. The rate of shoreline prop-

agation, i.e., regression rate, on the flanks is influenced by the rates of sea-level rise and sediment supply. The debouching of the Yellow River at around 1 ky BP dramatically increased the regression rate on the northern flank.

The incision of the Yangtze valley was primarily caused by sea-level fall because the area is located in a tectonic subsidence belt. The post-glacial fining-upward incised-valley fill was controlled by the retrogressive aggradation corresponding to the base-level rise. The upstream extent of the aggradation exceeded the extent of marine influence carried by tidal currents, explaining the lack of marine fossils and tidal sedimentary structures in the lower portion of the channel-fill sand facies. The studied stretch of the incised valley was likely located at least 230 km landward of the paleo-river mouth during the low stand of sea level. The times of marine flooding become progressively younger landward on the two flanks, and are also different from the flooding time of the incised valley. These result in diachronism in the stratigraphy of the Yangtze incised-valley system.

Acknowledgements

This research was supported by National Natural Science Foundation of China (Grant no. 49976016). We are grateful to Wu Meiyi for preparing the figures. Constructive earlier reviews were provided Drs. Harry H. Roberts, J.R. Suter, John Horne, E. Leithold, D.J. Stanley, and David Pepper. We thank Dr. Saito for sharing information on cores drilled recently in the Yangtze area.

References

Allen, G.P., Posamentier, H.W., 1993. Sequence stratigraphy and facies model of an incised valley fill: the Gironde Estuary, France. Journal of Sedimentary Petrology 63 (3), 378–391.

Belknap, D.F., Kraft, J.C., 1985. Influence of antecedent geology on the stratigraphic preservation potential and evolution of Delaware's barrier systems. Marine Geology 63, 235–262.

Borland, W.M., 1971. Reservoir sedimentation. In: Shen, H. (Ed.), River Mechanics, vol. II, pp. 29-1–29-38.

Chang, W.Y.B., 1996. Formation and evolution of the Taihu Lake since 11000a. Acta Palaeontologica Sinica 35 (2), 129–135 (in Chinese, with English abstract).

Chen, J., 1989. Topographical evolution of the Yangtze Estuary. In: Chen, J., Shen, H., Yu, C. (Eds.), Hydrodynamics and Geomorphological Evolution of the Yangtze Estuary. Shanghai Science and Technology Press, Shanghai, pp. 38–47.

Chen, Q., 1997. Characteristics and paleo-environmental implications of the Late Quaternary paleosols in the Yangtze Delta area. PhD Thesis, Marine Geology Department, Tongji University, no. 97002, 58 pp. (in Chinese, with English abstract).

Chen, X., 1998. Changjian (Yangtze) River delta, China. Journal of Coastal Research 14, 838–858.

Chen, Z., Chen, Z.L., 1997. Quaternary stratigraphy and trace-element indices of the Yangtze Delta, eastern China, with special reference to marine transgression. Quaternary Research 47, 181–191.

Chen, Q., Li, C., 1997. Pedogenesis and paleo-climatic implications of late Pleistocene paleosols in the Yangtze delta. In: Meco, Petit-Maire (Eds.), Climate of the Past. Servicio De Pullicaciones, Spain, pp. 43–49.

Chen, Z., Stanley, D.J., 1993. Yangtze delta, eastern China: 2. Late Quaternary subsidence and deformation. Marine Geology 112, 13–21.

Chen, Z., Stanley, D.J., 1995. Quaternary subsidence and river channel migration in the Yangtze delta plain, eastern China. Journal of Coastal Research 11, 927–945.

Cheng, X., 1987. Preliminary study on the live foraminifers in the surfacial sediment along the Yangtze River. Marine Geology & Quaternary Geology 7, 1–14 (in Chinese).

Coleman, J.M., 1988. Dynamic changes and processes in the Mississippi River delta. Geological Society of America Bulletin 100, 999–1015.

Coleman, J.M., Roberts, H.H., Stone, G.W., 1998. Mississippi River delta: an overview. Journal of Coastal Research 14, 698–716.

Dalrymple, R.W., Zaitlin, B.A., 1994. High-resolution sequence stratigraphy of a complex, incised valley succession, Cobequid Bay–Salmon River estuary, Bay of Fundy, Canada. Sedimentology 44, 1069–1091.

Dalrymple, R.W., Zaitlin, B.A., Boyd, R., 1992. Estuarine facies models: conceptual basis and stratigraphic implications. Journal of Sedimentary Petrology 62, 1130–1146.

Dalrymple, R.W., Boyd, R., Zaitlin, B.A., 1994. Incised-Valley Systems: Origin and Sedimentary Sequences. SEPM Special Publication No. 51, 391 pp.

Deng, B., Wu, G., Li, C., 1999. Paleo-climate recorded in the first layer of paleosol in the Yangtze Delta area. Marine Geology & Quaternary Geology 19 (3), 29–37 (in Chinese).

Fisk, N.H., 1944. Geological investigation of the alluvial valley of the lower Mississippi River. Technical Report, Mississippi River Committee, Vicksburg, Mississippi.

Fisk, H.N., McFarlan Jr., E., 1955. Late Quaternary deltaic deposits of the Mississippi River. Geological Society of America, Special Paper 62, 279–302.

Folk, R.L., 1974. Petrology of Sedimentary Rocks. Hemphill Publishing, Austin, TX, 182 pp.

Gessler, J., 1971. Aggradation and degradation. In: Shen, H. (Ed.), River Mechanics, vol. I, pp. 8-1–8-24.

Gupta, S., 1997. Tectonic control on paleovalley incision at the distal margin of the early Tertiary Alpine foreland basin, south-

eastern France. Journal of Sedimentary Research 67 (6), 1030–1043.
Gupta, S., 1999. Controls on sedimentation in distal margin palaeovalley in the Early Tertiary Alpine foreland basin, southeastern France. Sedimentology 4 (2), 357–384.
Li, C., 1984. Sedimentary processes in the Yangtze Delta since Late Pleistocene. Collected Oceanic Works 7 (2), 116–126 (in Chinese, with English Abstract).
Li, C., 1985. The Luanhe Fan-Delta Depositional System. Geological Publishing House, Beijing, 169 pp. (in Chinese).
Li, C., 1986. Deltaic sedimentation. In: Ren, M.E. (Ed.), Modern Sedimentation in Coastal and Nearshore Zone of China. China Ocean Press and Springer-Verlag, Beijing, Berlin, Heidelberg, New York, Tokyo, pp. 253–378.
Li, C., Li, P., 1983. Characteristics and distribution of Holocene sand bodies in the Yangtze delta. Acta Oceanologica Sinica 1 (2), 84–96 (in Chinese, with English abstract).
Li, C., Ming, Q., 1981. Holocene transgression and sea level change in the apical area of the Yangtze Delta. Journal of Tongji University 3, 104–108 (in Chinese, with English abstract).
Li, P., Sun, H., 1991. Paleosol characteristics in the late Quaternary strata of the Yangtze delta area. Shanghai Geology 1, 16–24 (in Chinese, with English abstract).
Li, C., Wang, P., 1991. Stratigraphy of the Late Quaternary barrier–lagoon depositional system along the coast of China. Sedimentary Geology 72, 189–200.
Li, C., Wang, P., 1998. Late Quaternary Stratigraphy of the Yangtze Delta. China Science Press, Beijing, 222 pp. (in Chinese).
Li, C., Zhang, G., 1997. Riverine sediments and Chinese coastline changes. Chinese Geographical Science 7 (3), 201–207 (in Chinese, with English abstract).
Li, C., Wang, J., Li, P., 1979. Preliminary study of the facies distribution in the Yangtze delta. Journal of Tongji University 3, 1–14 (in Chinese).
Li, C., Li, P., Chen, X., 1983. The influence of marine factors on the Yangtze River channel below Zhenjiang. Acta Geographica Sinica 38, 128–140 (in Chinese, with English abstract).
Li, C., Chen, G., Sun, H., 1988. Comparison study of delta systems in northern and southern China. Acta Sedimentologica Sinica 6 (1), 58–69 (in Chinese, with English abstract).
Li, C., Chen, G., Yao, M., Wang, P., 1991. The influences of suspended load on the sedimentation in the coastal zones and continental shelves of China. Marine Geology 96, 341–352.
Li, C., Chen, Q., Cong, Y., 1995. Late Quaternary paleosol and paleo-environment in Shanghai Area. Journal of Tongji University 23 (Supplementary), 165–171 (in Chinese, with English abstract).
Li, C., Chen, Q., Li, P., 1996. Late Quaternary buried paleosols and their parent materials in the Yangtze Delta. Journal of Tongji University 24, 439–444 (in Chinese, with English abstract).
Li, C., Zhang, J., Yang, S., Fan, D., 1999. Characteristics and paleoenvironment evolution of the tidal sand bodies in northern Jiangsu Province. Science in China, Series D 42 (1), 52–60.
Li, C., Chen, Q., Zhang, J., Yang, S., Fan, D., 2000. Stratigraphy and paleoenvironmental changes in the Yangtze Delta during the late Quaternary. Journal of Asian Earth Sciences 18, 453–469.
Li, C., Zhang, J., Fan, D., Deng, B., 2001. Holocene regression and the tidal radial sand ridge system formation in the Jiangsu coastal zone, east China. Marine Geology 173, 97–120.
Liu, B., 1993. Studies on the Late Quaternary paleosols in the Yangtze Delta area. PhD Thesis, Marine Geology Department of Tongji University, no. 93004, 75 pp. (in Chinese, with English abstract).
Liu, C., Wu, L., Cai, M., 1985. The depositional characteristics, origin and age of the cheniers in the south flank of the Changjiang (Yangtze) Delta. Acta Oceanologica Sinica 7 (1), 55–66 (in Chinese).
Makkaveev, N.E., 1960. Experimental Geomorphology. Moscow University Press, Moscow, 166 pp. (In Russian).
Martinson, D.G., Pisias, N.G., Hays, J.D., Imbrie, J., Moore, T.C., Shackleton, N.J., 1987. Age dating and the orbital theory of the ice age: development of a high-resolution 0 to 300,000-year chrono-stratigraphy. Quaternary Research 27, 1–29.
Milliman, J.D., Meade, R.H., 1983. World-wide delivery of river sediments to the oceans. Journal of Geology 91, 1–22.
Milliman, J.D., Syvitski, J.P.M., 1992. Geomorphic/tectonic control of sediment discharge to the ocean: the importance of small mountainous rivers. Journal of Geology 100, 525–544.
Nichol, S.L., Boyd, R., Penland, S., 1996. Sequence stratigraphy of a coastal-plain incised valley estuary: Lake Calcasieu, Louisiana. Journal of Sedimentary Research 66, 847–857.
Nichol, S.L., Zaitlin, B.A., Thom, B.G., 1997. The upper Hawkesbury River, New South Wales, Australia: a Holocene example of an estuarine bayhead delta. Sedimentology 44, 263–286.
Oomkens, E., 1970. Depositional sequences and sand distribution in the postglacial Rhone delta complex. In: Morgan, J.P., Shaver, R.H. (Eds.), Deltaic Sedimentation: Modern and Ancient, SEPM Special Publication No. 15, pp. 312–345.
Oomkens, E., 1974. Lithofacies relations in the Late Quaternary Niger Delta complex. Sedimentology 21, 195–222.
Posamentier, H.W., Vail, P.R., 1988. Eustatic controls on clastic sedimentation: II. Sequence and systems tract models. In: Wilgus, C.K., Hasting, B.S., Posamentier, H.W., Ross, C.A., van Wagoner, J.C., Kendall, C.G.St.C. (Eds.), Sea-Level Change: An Integrated Approach. SEPM Special Publication No. 42, pp. 125–154.
Posamentier, H.W., Jervey, M.T., Vail, P.R., 1988. Eustatic controls on clastic sedimentation: I. Conceptual framework. In: Wilgus, C.K., Hasting, B.S., Posamentier, H.W., Ross, C.A., van Wagoner, J.C., Kendall, C.G.St.C. (Eds.), Sea-Level Change: An Integrated Approach. SEPM Special Publication No. 42, pp. 109–124.
Qian, N., Li, G., Xie, H., Zhou, Z., 1964. Sand body formation in the Qiantangjiang Estuary. Acta Geographica Sinica 30 (2), 124–142 (in Chinese, with English abstract).
Qian, N., Zhang, R., Zhou, Z., 1989. Evolution of River Channel. China Science Press, Beijing, 584 pp. (in Chinese).
Qin, Y., Zhao, Y., Chen, L., 1987. Geology of East China Sea. Science Press, Beijing, 274 pp. (in Chinese).
Reineck, H.E., Singh, I.B., 1980. Depositional Sedimentary Environments. Springer-Verlag, New York, 549 pp.
Ren, M., 1986. Comprehensive Investigation of Coastal Zone and Tidal Flat Resources, Jiangsu Province. China Ocean Press, Beijing, 517 pp. (in Chinese).

Roberts, H.H., 1997. Dynamic changes of the Holocene Mississippi River delta plain: the delta cycle. Journal of Coastal Research, 605–627.

Roy, P.S., 1984. New South Wales estuaries: their origin and evolution. In: Thom, B.G. (Ed.), Developments in Coastal Geomorphology. Australia Academy Press, Sydney, pp. 99–121.

Roy, P.S., 1994. Holocene estuary evolution-stratigraphic studies from southern Australia. In: Dalrymple, R.W., Boyd, R., Zaitlin, B.A. (Eds.), Incised-Valley Systems: Origin and Sedimentary Sequences. SEPM Special Publication No. 51, pp. 241–263.

Roy, P.S., Cowell, P.J., Thom, B.G., 1995. Wave-dominated coasts. In: Cater, R.W.G., Woodroffe, C.D. (Eds.), Coastal Evolution. Cambridge Univ. Press, pp. 121–186.

Russell, R.J., Russell, R.D., 1939. Mississippi River delta sedimentation. In: Trask, P.D. (Ed.), Recent Marine Sediments. American Association of Petroleum Geologists, pp. 153–177.

Said, R., 1981. The River Nile. Springer-Verlag, Berlin, 151 pp.

Saito, Y., 1998. Sea level since Last Glacial Period in the continental shelf of the East China Sea. Quaternary Research 37 (3), 235–242 (in Japanese, with English abstract).

Shen, Y., Huang, D., Qian, C., 1993. Preliminary illustration of formational mechanism of semidiurnal tidal wave system in the Yellow Sea. Acta Oceanologica Sinica 15 (6), 15–24 (in Chinese, with English abstract).

Simons, D.B., Senturk, F., 1977. Sediment Transport Technology. Water Resources Publications, Fort Collins, CL, pp. 750–754.

Stanley, D.J., 1996. Nile delta: extreme case of sediment entrapment on a delta plain and consequent coastal land loss. Marine Geology 129, 189–195.

Stanley, D.J., Bernasconi, M.P., 1998. Relict and palimpsest depositional patterns on the Nile shelf recorded by molluscan faunas. Palaios 13, 79–86.

Stanley, D.J., Chen, Z., 1993. Yangtze delta, eastern China: 1. Geometry and subsidence of Holocene depocenter. Marine Geology 112, 1–11.

Stanley, D.J., Warne, A.G., 1998. Nile delta in its destruction phase. Journal of Coastal Research 14, 794–825.

Suter, J.H.L., Berryhill Jr., H.L., Penland, S. 1987. Late Quaternary sea-level fluctuations and depositional sequences, southwest Louisiana continental shelf. In: Nummedal, D., Pilkey, O.H., Howard, H. (Eds.), Sea-Level Fluctuation and Coastal Evolution. SEPM Special Publication No. 41, pp. 199–219.

Van Wagoner, J.C., Posamentier, H.W., Mitchum, R.M., Vail, P.R., Sarg, J.F., Loutit, T.S., Hardenbol, J., 1988. An overview of the fundamentals of sequence stratigraphy and key definitions. In: Wilgus, C.K., Hasting, B.S., Posamentier, H.W., Ross, C.A., Van Wagoner, J.C., Kendall, C.G.St.C. (Eds.), Sea-Level Change: An Integrated Approach. SEPM Special Publication, No. 42, pp. 39–45.

Van Wagoner, J.C., Mitchum, R.M., Campion, K.M., Rahmanian, V.D., 1990. Siliciclastic sequence stratigraphy in well logs, cores, and outcrops: concepts for high-resolution correlation of time and facies, AAPG Methods in Exploration Series, No. 7 Tulsa, Oklahoma, 55 pp.

Wang, P., 1985. Marine Micropaleontology of China. China Ocean Press and Springer-Verlag, Beijing, Berlin, New York, 370 pp.

Wang, Y., 1993. Report on evolution of past building conditions in Wanggan Area, Jiangsu Province. Technical Report of Nanjing University (in Chinese).

Wang, J., Sha, R., Wang, Y., Xiao, J., Znou, C., Hu, X., Chen, G., Huang, X., 1997. Coastal development and environmental evolution in central part of Jiansu Province derived from a long drilling section. Acta Sedimentologica Sinica 15 (Supplementary), 51–56 (in Chinese with English abstract).

Wang, Y., Zhu, D., Zhou, L., Wang, X., Jiang, S., Li, H., Shi, B., Zhang, Y., 1998. Sedimentary characteristics and evolution if the radial tidal sand ridges in southern Yellow Sea. Science in China, Series D 28, 385–393.

Wilkinson, B.H., Byrne, J.R., 1977. Lavaca Bay transgressive deltaic sedimentation in central Texas Estuary. AAPG Bulletin 64 (4), 527–545.

Wright, L.D., Coleman, J.M., 1972. River delta morphology: wave climate and the role of the subaqueous profile. Science 176, 282–284.

Wu, L., Liu, C., 1989. Sedimentological characteristics and age of the Pleistocene stiff mud in the Shanghai area. Oceanology of the East China Sea 7, 73–79 (in Chinese).

Zaitlin, B.A., Dalrymple, R.W., Boyd, R., 1994. The stratigraphic organization of incised-valley systems associated with relative sea-level change. In: Dalrymple, R.W., Boyd, R., Zaitlin, B.A. (Eds.), Incised-Valley Systems: Origin and Sedimentary Sequences. SEPM Special Publication No. 51, pp. 45–62.

Zhang, G., Li, C., 1996. The fills and stratigraphic sequences in the Qiantangjiang incised paleovalley, China. Journal of Sedimentary Research 66 (2), 406–414.

Zhang, J., Li, C., Cong, Y., 1998. Hydrodynamic environment and sediment source of the tidal sand ridges in the Jiangsu Coast Plain. Acta Oceanologica Sinica 20 (3), 82–90 (in Chinese with English abstract).

Zhao, J., Li, C., Zhang, G., 1997. Discovery of the tidal sand body area in northern flank of the Yangtze Delta and its geological significance. Journal of Tongji University 25, 82–86 (in Chinese with English abstract).

Zhu, Y., Li, C., Zeng, C., 1979. On late Pleistocene low stand of sea level in East China Sea. Chinese Science Bulletin 24 (7), 317–320 (in Chinese).